NGU REPORT 2020.030

Knipovich Ridge Aeromagnetic Survey 2016: processing and interpretation

GEOLOGY FOR SOCIETY

SINCE 1858

GEOLOGICAL SURVEY OF NORWAY

- NGU -

NORGES GEOLOGISKE UNDERSØKELSE
· NGU ·

REPORT

Geological Survey of Norway
P.O.Box 6315 Torgarden
NO-7491 TRONDHEIM
Tel: 47 73 90 40 00

Report no.: 2020.030

ISSN: 0800-3416 (print)
ISSN: 2387-3515 (online)

Grading: Open

Title:
Knipovich Ridge Aeromagnetic Survey 2016: processing and interpretation

Authors: Marie-Andrée Dumais, Odleiv Olesen, Laurent Gernigon, Marco Brönner, Anna Lim (NTNU), Ståle Johansen (NTNU)

Client:
EPOS-N, NGU, NPD

County:

Commune:

Map-sheet name (M=1:250.000)

Map-sheet no. and -name (M=1:50.000)

Deposit name and grid-reference:

Number of pages: 45 **Price (NOK):** 160
Map enclosures:

Fieldwork carried out:
30.08.2016 -
. 11.09.2018

Date of report:
01.10.2020

Project no.:
369700

Person responsible:
Jostein Mårdalen
Jostein Mårdalen

Summary:
As an ultra-slow spreading ridge in an oblique system located between the Svalbard - Barents Sea and the Northeast Greenland rifted margins, the dynamics of the Knipovich Ridge opening has long been debated. Its 90-degree bend with the Mohn's Ridge, rare in plate tectonics, affects the evolution of the Fram Strait and motivates the study of crustal deformation with this distinctive configuration.

This report comprises the results of the Knipovich Ridge Aeromagnetic Survey 2016 project. Aeromagnetic data were acquired and processed in the Fram Strait on the western coast of Svalbard encompassing the Knipovich Ridge. The aeromagnetic data were merged to data available in the surrounding areas.

For the first time, magnetic isochrons related to the spreading of the Knipovich Ridge have been identified. They indicate a spreading initiation at C6 (~20 Ma) and a ridge jump at C5E (~18 Ma). These results were used to reconstruct the plate tectonic development of the area.

A 3-D magnetic inversion modelling was also performed on the KRAS-16 aeromagnetic data and compared to the high-resolution bathymetry acquired in the rift valley by the NPD. The higher magnetization was correlated to the presence of volcanic features and bathymetric highs.

A 2-D forward modelling was done with available global gravity data compilation, seismic interpretation, and a CSEM / MT profile. From the 2-D modelling interpretation, the crustal domains are delineated and confirmed with the Werner deconvolution and the Curie point depth estimation. The continent-ocean boundary (COB) on the east margin is relocated up to 160 km to the west of the location set by previous studies. Therefore, the mapped extent of the oceanic domain is considerably reduced. A wide transition lithospheric domain is also delineated, most likely comprising an exhumed lower crust or mantle.
The project was conducted at NGU with financial contribution from the NFR funded EPOS-N project, Geological Survey of Norway (NGU) and Norwegian Petroleum Directorate (NPD

OLJEDIREKTORATET

GEOLOGICAL SURVEY OF NORWAY · NGU ·

EPOS-N EUROPEANPLATEOBSERVINGSYSTEM - NORWAY

Keywords: Aeromagnetic	Fram Strait	Knipovich Ridge
Plate reconstruction	Modeling	Crustal domains
Gravity	EM	Scientific report

Contents

1 Introduction

The Knipovich Ridge Aeromagnetic Survey 2016 (KRAS-16) is an initiative to map the ultraslow spreading ridge in the Fram Strait and the surrounding area with airborne magnetic measurement.

Aeromagnetic surveys are essential for detailed mapping of continent-ocean boundaries (COB), magnetic spreading anomalies, faults, fracture systems, lava flows and magmatic intrusions. The KRAS-16 survey represents the missing piece in the Norwegian-Greenland Sea puzzle and enables us to produce a complete map the complex system of abandoned (or extinct) spreading ridges and fracture zones in this area. A geodynamic interpretation of the new aeromagnetic compilation will facilitate a first order dating of the opening of the Fram Strait and the transition from a transform fault to a spreading ridge. The characteristic striped pattern of magnetic spreading anomalies is an imprint of the Earth's magnetic field reversals and therefore act as a timeline record of opening of the Arctic Ocean.

The magnetic signature of the spreading ridge also reveals the geological framework of the Fram Strait development and gives insights of the tectonic settings of the Northeast-Greenland and Svalbard-Barents Sea margins. Furthermore, aeromagnetic interpretation allows us to model the continent-ocean transition, estimate the depth-to-basement and to characterize the basement types.

2 Survey Characteristics and Acquisition

The Knipovich Ridge spreading history and the development of the Fram Strait are the main goals of the present study (Figure 1). Classified as an ultraslow-oblique spreading system (with spreading rates of less than 20 mm/year), the Knipovich Ridge comprises the Arctic Mid-Ocean Ridge system delimited by the Mohn's Ridge (~73°50' N) and Molloy Fracture Zone (~78°30' N) between Greenland and NE Atlantic oceanic realms. The Knipovich Ridge trends from NW in the south to N in the north with a 130 km-wide escarpment and largely covered with thick piles of sedimentary rocks along the Svalbard margin (Engen et al., 2006). Its tectonic structure differs from other oceanic ridges as it presents ultra-slow spreading features in an oblique system (Talwani & Eldholm, 1977; Vogt et al., 1982). The Fram Strait developed after a Late Cretaceous-Eocene rifting event between the Barents Sea and the Northeast Greenland. It forms a complex system of conjugate shear margins characterized by distinct crustal, structural and magmatic properties (Faleide et al., 2008; Ritzmann & Jokat, 2003; Srivastava & Roest, 1999). During the Paleocene-Eocene, the oblique system underwent a brief period of compression leading to the Eurekan-Spitsbergen fold and thrust belts (Piepjohn et al., 2016). The importance of this study is to delineate the continent-ocean boundary, determine the crustal domains and map the spreading of the ridge. The settings and timing of the Fram Strait opening contribute to the geological framework of the Greenland and Svalbard-Barents Sea margins.

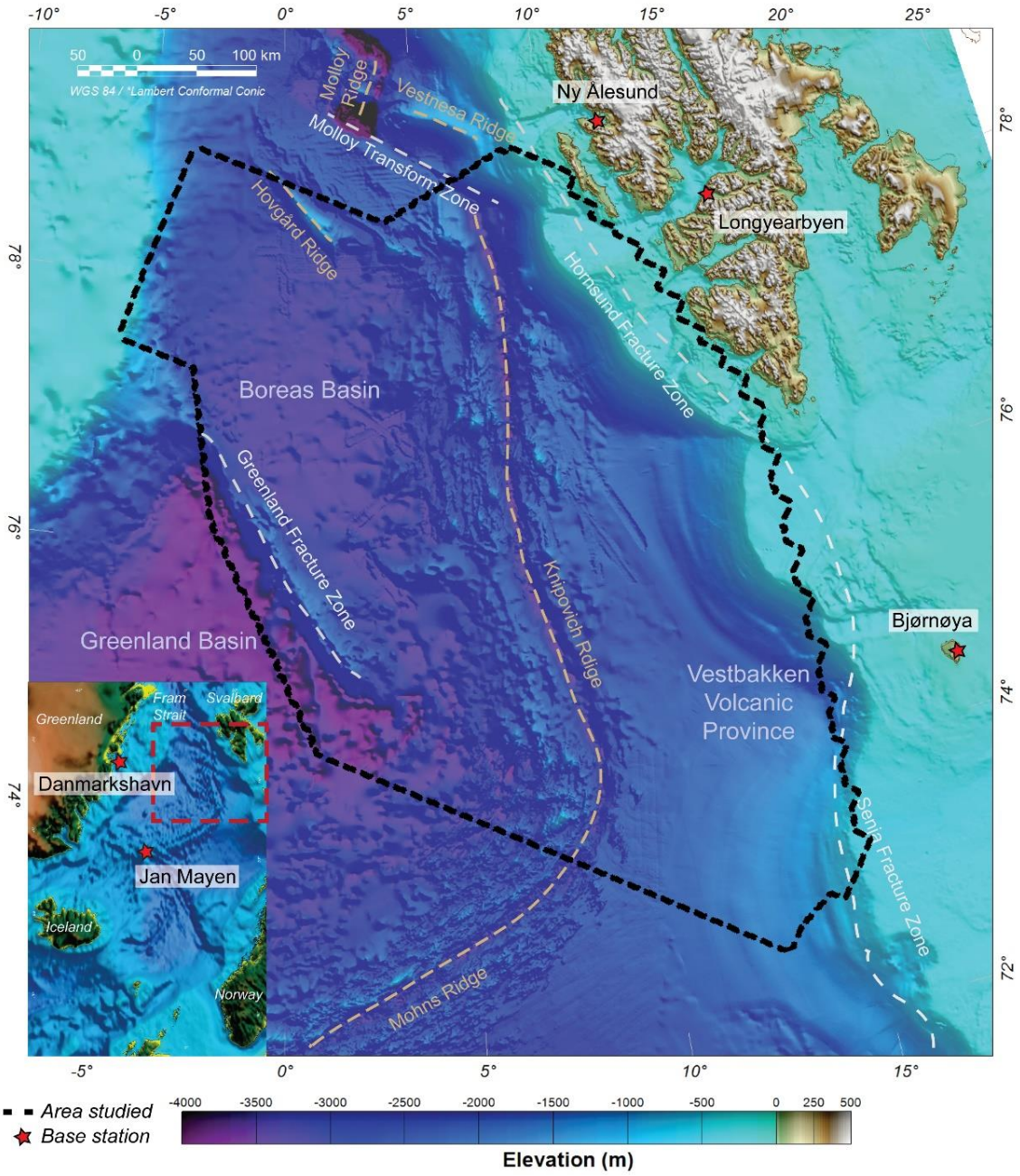

Figure 1. Survey area with magnetic stations available (Bjørnøya, Danmarkshavn, Jan Mayen, Longyearbyen and Ny Ålesund)

2.1 Survey Area and Survey Parameters

The survey area is 254,000 km^2, with a total of 56,906 line-km flown, 5.5 km line spacing and oriented 120-300° – perpendicular to the spreading anomalies. The acquisition took place during the two summers of 2016 and 2018 due to technical difficulties to fly the area.

Survey specifications	
Survey area	254,000 km^2
Survey size	56,906 line-km
Line direction	120-300°
Tie-line direction	30-210°
Line spacing	5.5 km
Tie-line spacing	20 km
Acquisition – phase 1	August 30th to October 6th, 2016
Acquisition – phase 2	May 26th to September 9th, 2018

2.2 Instrumentation and Technical Specifications

A concise description of the instruments on-board of the aircraft is found in the operation report provided by Novatem (Novatem, 2018).

Diurnal variation of the magnetic field was monitored before and during the flights. The magnetic base stations used were Ny Ålesund, Longyearbyen, Bjørnøya and Jan Mayen, operated by the Tromsø Geophysical Observatory (http://flux.phys.uit.no) and Danmarkshavn, operated by the Technical University of Denmark (http://www.space.dtu.dk). They constitute the closest magnetic observations available near the survey area (Figure 1).

2.3 Survey Operations

Survey operations were carried out by Novatem. A description is found in the operation report in (Novatem, 2018). Summary of the operations are found in the weekly reports produced by NGU (Appendix A).

Figure 2. The aircraft over the Svalbard margin (curtesy of Novatem, Inc)

3 Data Processing

Processing of the data were carried out at NGU using the raw compensated data from Novatem with their proprietary methods as described in the acquisition report (Novatem, 2018).

3.1 Line Correction and De-spiking

The compensation filter is usually effective to remove noise generated by the aircraft and the engines. Small residual noise (0-3 nT) occurring from radio-communication or any external electro-

magnetic source can be manually adjusted (Figure 3). L1061-1 is the only line that required manual adjustment.

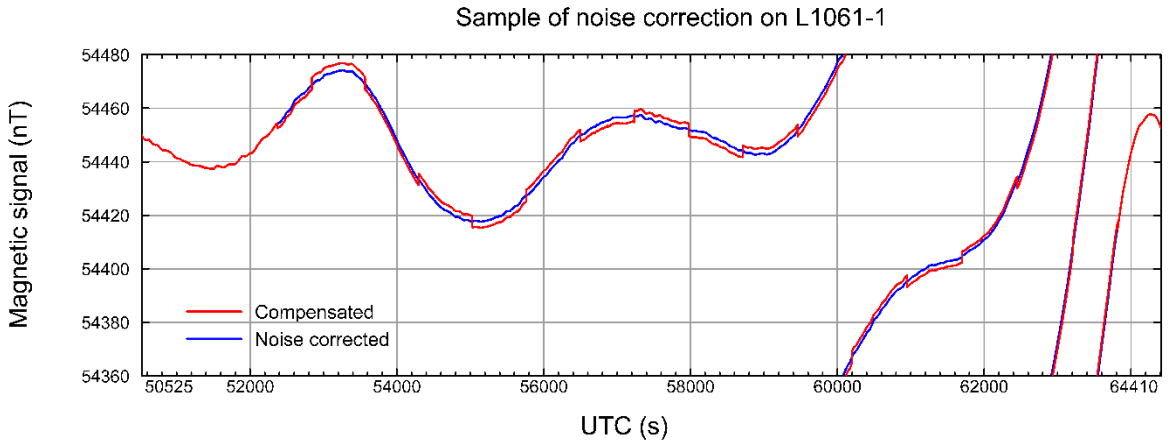

Figure 3. Sample data from L1061-1. Manual adjustment was carried on the data to remove external noise of 3 nT amplitude

3.2 IGRF

Long temporal variations of the inclination, declination, and field intensity, called secular variations, are important to consider for this survey which was flown over a long period during two non-consecutive summers. Therefore, the magnetic anomaly signal is calculated by subtracting the 12th International Geomagnetic Reference Field (IGRF-12) model, which is reliable to estimate secular variations.

3.3 Diurnals Correction

Located at high latitude, the survey area is particularly sensitive to diurnal noise. Frequent polar magnetospheric substorms cause large disturbances of the Earth's magnetic field and propagate diurnal noise over a large area with significant temporal and spatial variations. Substorms are transient processes causing disturbances of 300-800 nT of the horizontal field component over 0.5-3 hr. The aeromagnetic data acquired for KRAS-16 were acquired during low to moderate solar cycle activity optimizing the data quality.

3.3.1 Base Stations Monitoring

The diurnal noise was carefully assessed during the acquisition and processing steps. Five magnetic base stations from the Tromsø Geophysical Observatory (TGO) and the Technical University of Denmark (DTU) were closely monitored to provide a global overview of the magnetic activity in real time and were used for the data post-processing. This ensures high confidence and reliability of the final dataset products, representing the true geophysical nature of the Knipovich Ridge and its surroundings.

As an example, on September 1st, 2016, a flight was flown late during the day (Figure 4a). All base stations showed a very quiet magnetic activity until 20:00 (UTC) when the onset of polar magnetospheric substorms occurred. Figure 4a indicates how the time of the onset varied from one station to the other. It is also noticed that the amplitude of the horizontal deviation varies depending on the location of the base station. Figure 4b shows the profile as acquired and compared to a re-flight. The response is significantly different with ~300 nT difference in some areas. The

profile was first corrected with the base station of Jan Mayen and then compared to a correction with the base station of Longyearbyen. The line was flown from NW to SE, from the Greenland margin towards Svalbard. Near Svalbard, Longyearbyen diurnal corrections are more effective to correct the profile. Further west, Jan Mayen is more suitable to correct the profile. No base station is particularly efficient in the centre of the profile. Hence, the diurnal correction was carried with caution.

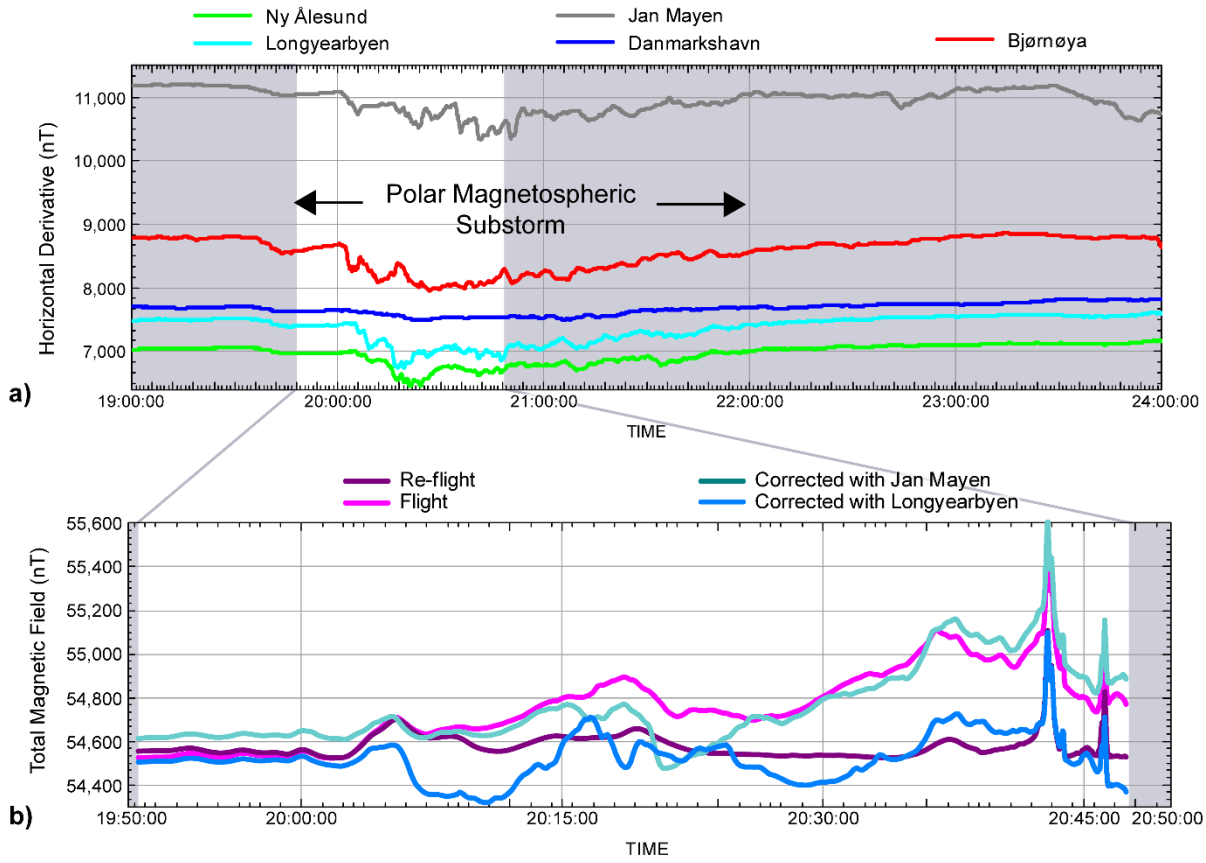

Figure 4. a) Magnetic recordings at five observatories during acquisition of the L1081 profile flown on September 1st, 2016 in a polar magnetospheric substorm b) profiles corrected with different base stations and compared to a re-flight.

3.3.2 Base Station Corrections

The data from the base station were collected at 1Hz and interpolated to the data sampling (10 Hz). For each base station, the average over the duration of the survey acquisition phase was removed to allow the correction of the long trend noise along the lines.

3.3.3 USGS Planar Interpolation

The USGS GX software package (Phillips, 2007) was used to correct for the diurnal noise. The module allows up to 5 stations to be used simultaneously and calculate a weighted average based on the inverse distance of the base station to the location of the measurements.

No base station correction was applied to profile L1008.0 as there was a weak correlation between the base station data and the flight data.

3.4 Levelling

The levelling was performed using the Geosoft Statistical Level module for the tie lines (Geosoft, 2010). For each tie line, this function calculates an average difference between the tie line values and the cross-over of the survey lines. Then it applied this average difference to shift each individual tie-line.

The second phase of the levelling was made using Geosoft Spline Level module (Geosoft, 2010). In this step, the tie lines are assumed to be properly levelled. Only the survey lines are corrected to match the levelled tie lines at each intersection. Several intersections corrections were manually adjusted or removed to allow a smooth and realistic levelling. A smooth Akima spline interpolation was applied to the correction to improve the levelling.

3.5 Micro-levelling

In order to remove the faint linear trend along the lines, one micro-levelling pass was applied to the dataset. The noise was first extracted from the gridded data using a decorrugation cut-off wavelength of 11,000 m for 5,500 m line spacing. Afterwards, a Naudy filter of 1,000 fiducials was applied to the profiled data. The final dataset is presented in Figure 5.

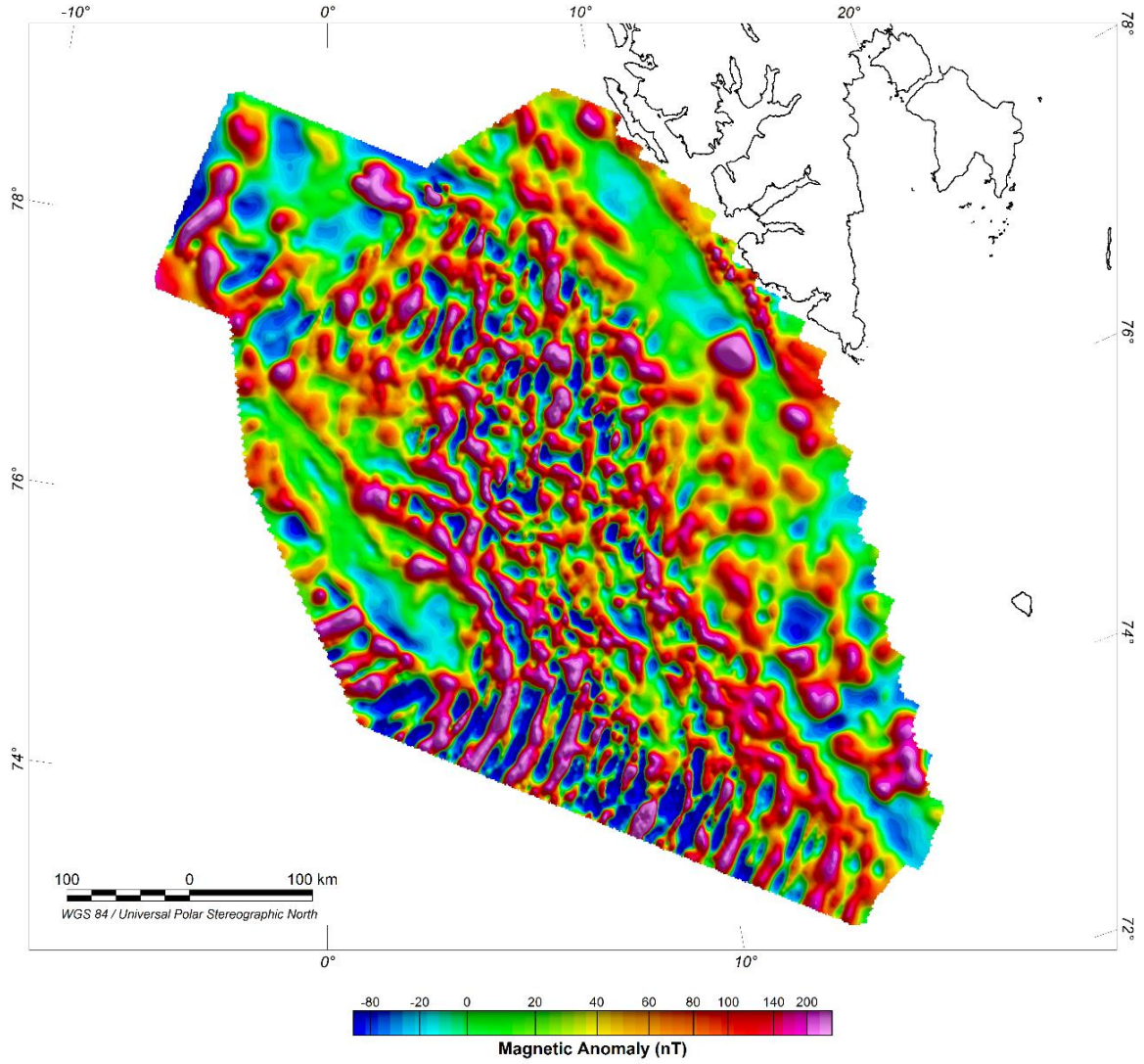

Figure 5. Processed magnetic data including base-station correction, levelling, and micro-levelling

4 Data Compilation

The KRAS-16 aeromagnetic dataset was gridded and merged with the available data in the surrounding areas. The surrounding areas are a compilation previously made for the EPOS-N project consisting of the publicly available datasets from the Arctic Circum Magnetic Map (Gaina et al., 2011). The data were upward continued to 1 km and the grid cell size is 2000 m.

The KRAS-16 aeromagnetic data generally fit with the surrounding data except in the Boreas Basin on the northwest corner of KRAS-16. Proprietary TGS data (Trulsvik et al., 2011) show significant differences in that area due to higher resolution and prove a better fit with the KRAS-16 aeromagnetic data.

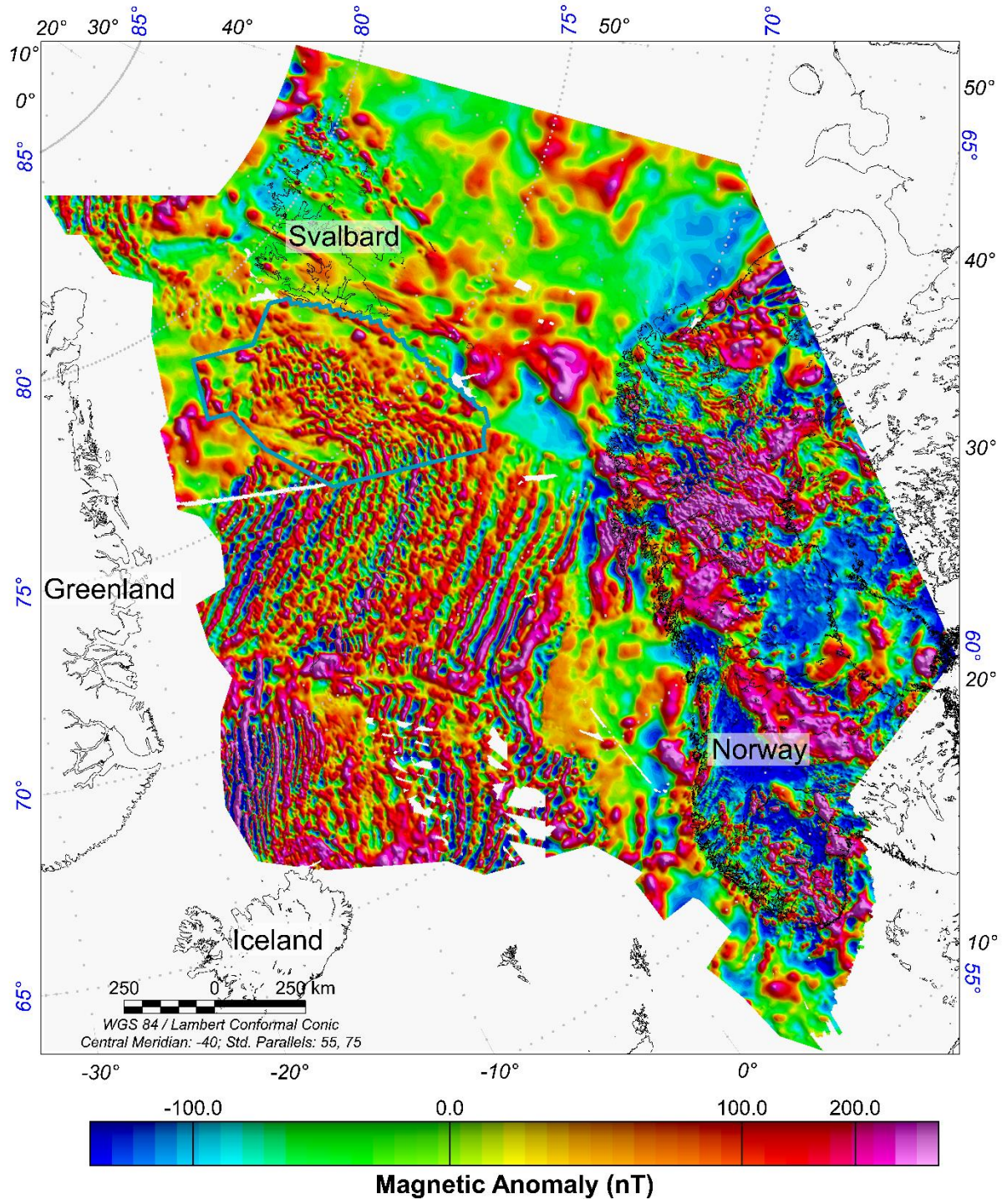

Figure 6. Magnetic anomaly compilation including the new KRAS-16 dataset

5 Interpretation

5.1 Interpretation of the Spreading Anomalies

The *ModMag* software (Mendel et al., 2005) was used to map the spreading of the sections (spreading fragments) identified along profiles A and B in Figure 7. These sections were chosen as they represent a continuous and full spreading sequence. The interface allows the user to perform a forward modelling of a specific spreading pattern, giving rate and asymmetry values, and then compare the result with the observed data. Profile A was initially tested for 5 km full crustal

thickness (Figure 7a). However, oceanic crust is in a first order divided in relatively lower magnetic gabbros and high magnetic basalts on top. An upper crust of a constant 1 km thickness (Johansen et al., 2019), representing the high magnetic basalt layer 2A, was then chosen to improve the agreement with the observed anomaly. Spreading rates and their respective asymmetries are also provided to build the forward model. Since the magnetic signature is continuous from Mohn's Ridge to Knipovich Ridge at the bend, initial identification of the magnetic isochrons were derived from the Mohn's Ridge interpretation (Engen et al., 2008; Vogt et al., 1986) to model Profile A consistently. This is only possible as the magnetic signature is continuous from one ridge to the other. All parameters are adjusted by iteration to fit the observed data. To ensure a data fit with the model, the sediment thickness was estimated from Engen et al. (2006).

In the magnetic data (Figure 8), domains consisting of high-frequency striped magnetic anomalies delineate the oceanic domain, characterized by magnetized basalt and magnetic isochron correlated to the chronostratigraphic chart of Ogg (2012). Following the interpretation of profiles A and B, magnetic isochron C6 is assigned to the first unambiguous striped anomaly. C5A, C5 and C1 are also assigned as they extend continuously from the Mohn's Ridge to the Knipovich Ridge. Modelling with 1 km upper crustal thickness instead of 5 km requires higher magnetization but replicates the higher frequency magnetic isochrons with higher confidence. Additionally, the dataset captures previously unresolved magnetic isochrons e.g. C2A, facilitating a more detailed and better constrained plate reconstruction. These also characterize the oceanic domain, where C6 demarks the first unambiguous magnetic isochron and revise the location of the expected continent-ocean boundary (COB) landwards of C6. Unlike the Mohn's Ridge, the Knipovich Ridge magnetic signature suggests the presence of several asymmetrical discontinuous spreading segments (Figure 8). Yet unobserved on bathymetric data, these new oceanic transfer faults are delineated, running parallel to the Greenland Fracture Zone and the Molloy Transform Zone (Figure 1) but perpendicular to the spreading anomalies. The spreading-stripe anomalies are not always continuous along the ridge, indicating segments of the spreading system often separated by these oceanic fracture zones. This highlights the segmented nature of the spreading system. Furthermore, some of these segments experience strong asymmetrical spreading, while others show small amplitudes and low magnetization (Figure 8), which underlines the complexity and heterogeneity of this ultra-slow spreading system in a sheared setting. The bathymetric data indicate that the Knipovich Ridge is trending from 347°, at the junction with Mohn's Ridge, to 002°, at the Molloy Transform Zone junction (Curewitz et al., 2010). On the magnetic data, the direction of the visible spreading anomalies is 300° (Figure 8). With the stable plate motion direction and the ridge trend propagation, the obliquity varies from ~45°, at Mohn's Ridge, to ~30°, at Molloy Transform Zone. The thick sedimentary cover of the Barents Sea fan (Engen et al., 2006) on the eastern flank of Knipovich Ridge causes lithospheric flexure and isostatic adjustment means that the magnetic sources in the crust are further away from the magnetic measurements, this causes the presence of wider anomalies and lower frequencies compared to their conjugate. According to the model, the extent of the spreading anomalies remains slightly asymmetric, implying the spreading evolution with moderately faster rates towards east at the bend connecting Mohn's Ridge and Knipovich Ridge (Figures 777 and 8). Between profile A and B, the spreading rates decrease east of Knipovich Ridge, while they appear to keep similar rates on the western side (Figure 7). Thus, around N76°, the asymmetry reverses, and the western oceanic domain becomes apparently larger.

Consequently, the segment between N76° and N78° reveals a pronounced asymmetry with a broader extent of the oceanic domain west of the present-day Knipovich Ridge (Figures 7 and 8). The new magnetic data indicate the presence of an atypical and failed spreading system, immediately west of the current ridge and east of the continental Boreas Basin, explaining the evident asymmetry of the spreading. The abandoned ridge model is favoured over a model with one single highly asymmetric system. The latter model would require much faster spreading towards the west, an unequal number of magnetic isochrons on either side of the ridge, and very different spreading rates from north to south. While there is no evidence of a failed spreading system in the bathymetry due to the sediment cover, the top crustal basement interpreted by Hermann and Jokat (2013) supports the presence of a separated basin or a rift valley. Thus, the failed spreading system with a ridge jump hypothesis was tested along profile B located in the most asymmetric segment of the Knipovich Ridge. The final model presents slower spreading rates particularly towards the east and confirms the presence of an atypical oceanic domain initiated at C6. In addition, it suggests a ridge jump between C5E and C5C, required to explain this asymmetry (Figures 7 and 8).

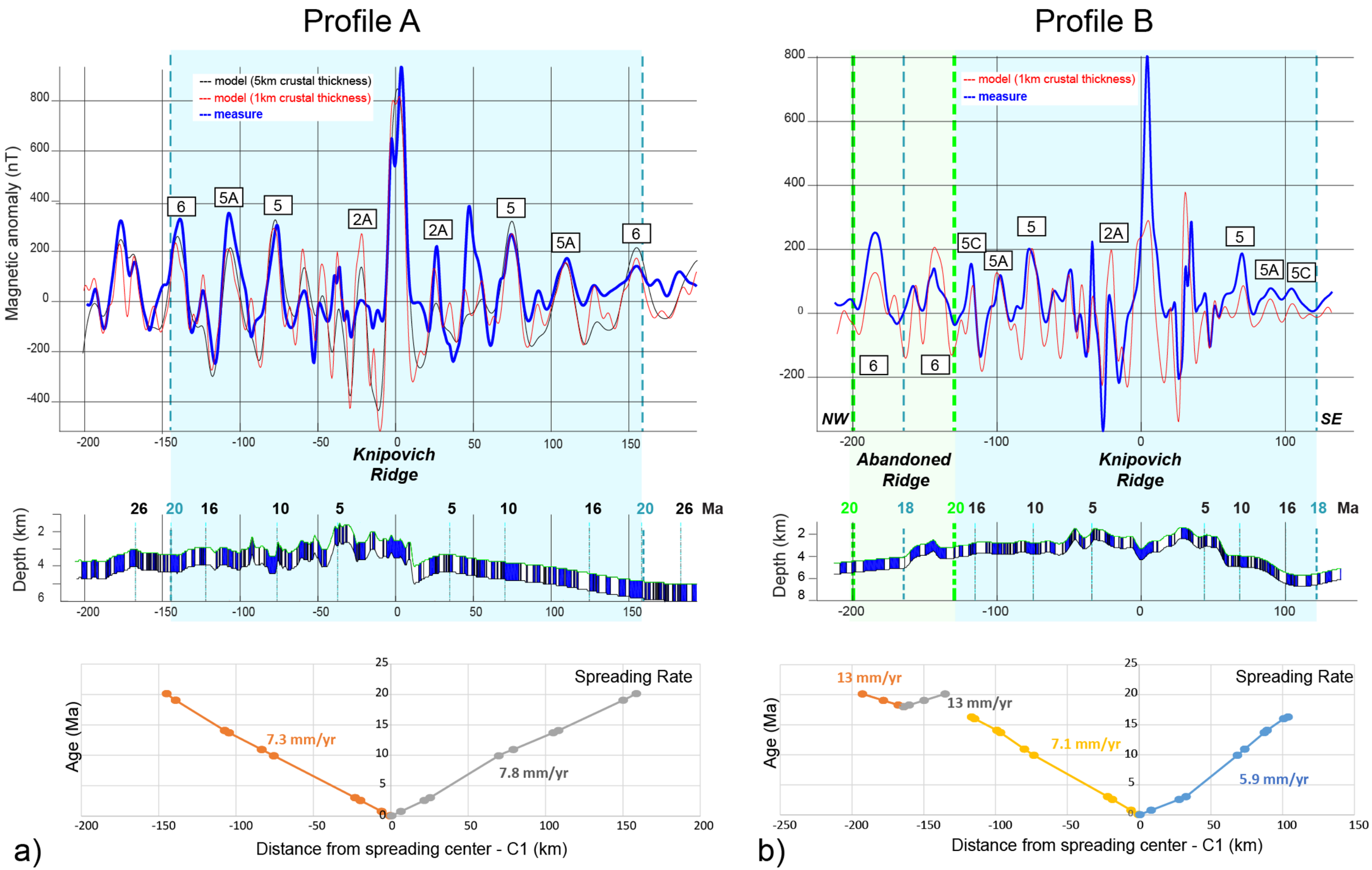

Figure 7. a) and b) Profiles A and B models, respectively, of the spreading rates. An abandoned ridge is modelled on Profile B to explain the magnetic isochron present along the profile (Dumais et al., accepted).

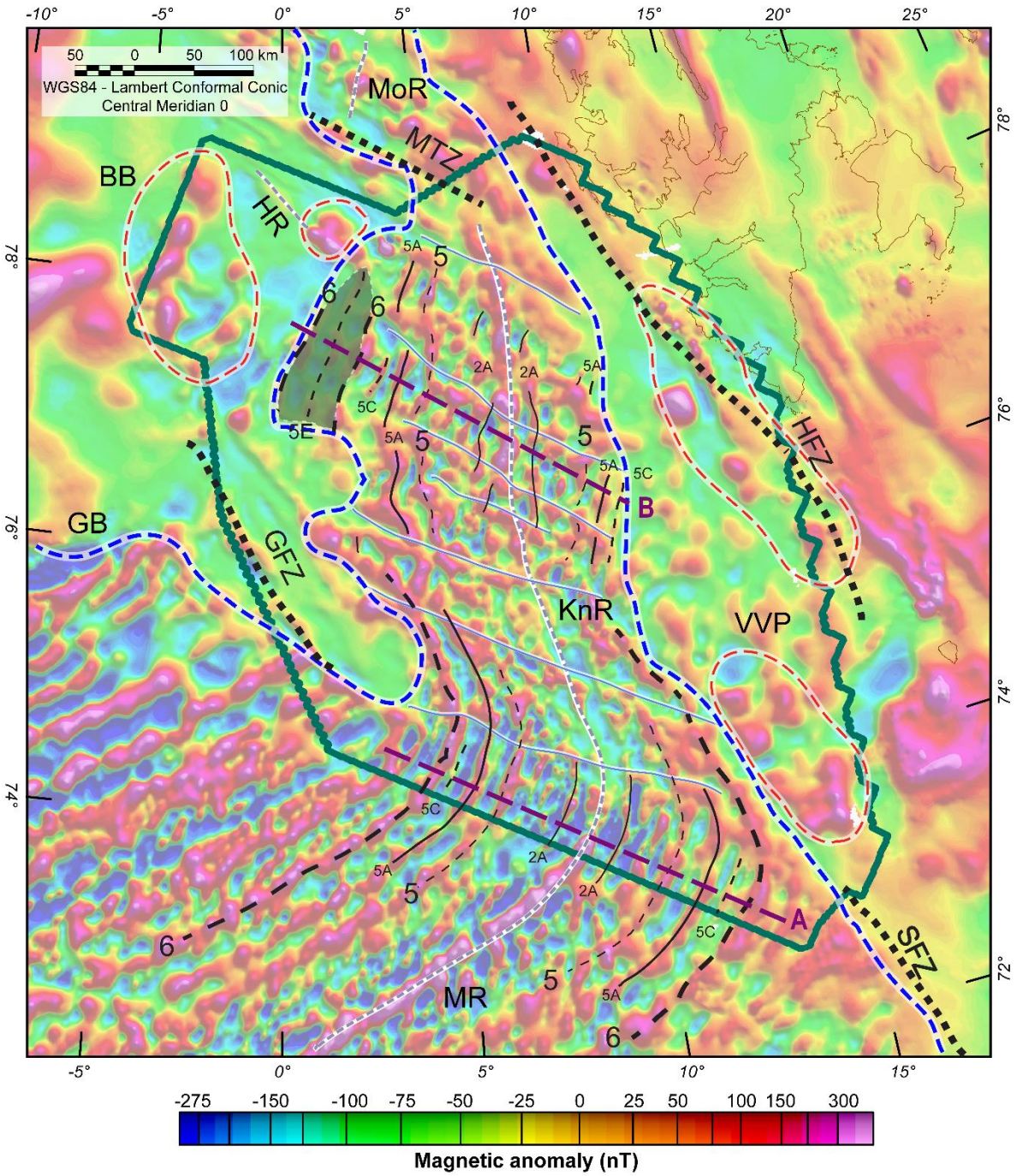

Figure 8. Magnetic interpretation (Dumais et al., accepted). The new aeromagnetic data revealed the timing of the breakup (C6) and magmatic events on the eastern side of the ridge. Profiles A and B are in purple. MoR: Molloy Ridge, MTZ: Molloy Transform Zone, HR: Hovgaard Ridge, BB: Boreas Basin, HFZ: Hornsund Fracture Zone, KnR: Knipovich Ridge, GFZ: Greenland Fracture Zone, GB: Greenland Basin, JMMC: Jan Mayen Microplate Complex, VVP: Vestbakken Volcanic Province, MR: Mohn's Ridge, SFZ: Senja Fracture Zone. New oceanic fracture zones are displayed with white lines, new COB demarcation is in dashed blue line and atypical volcanic areas are delimited by the dashed red polygons. An abandoned spreading ridge is highlighted in grey shading.

5.2 Reconstruction

Plate reconstruction was carried out using the open-source *Gplate 2.2 software* (Müller et al., 2018). The interface allows the visualization and the manipulation of the plate-tectonic reconstruction. Features are input in the software such as coastlines, plate boundaries and isochron files (Gernigon et al., 2019; Matthews et al., 2016). The plate boundary and the magnetic anomaly picks defined in

the Fram Strait are input in the feature collection. An age is assigned to the magnetic anomaly picks estimated from the modelling performed with the *ModMag software* (Mendel et al., 2005). Geometries are edited to allow the formation and cessation of the abandoned spreading ridge, to the west of the present-day Knipovich Ridge.

In the plate reconstruction of the Fram Strait (Figure 9), the spreading initiated at C6 (20 Ma). Around 18 Ma (C5E-C5C), the section between N77° and N78° is abandoned and migrates to the east where the spreading continues, forming today's Knipovich Ridge (Figure 9). Within this new section, the spreading becomes faster towards the Boreas Basin. Between N75° and N76°, the striped anomalies disappear ridgewards of C5 (10 Ma), implying relatively low magnetic crust, which need further investigation. The segment linking the Molloy Transform Zone shows a magnetic isochron corresponding to C1, with no further striped anomalies parallel to it, suggesting an opening more recent than C2A. The oceanic fracture zones observed appear to delimit the spreading segments in terms of abandoned ridge and migration, poor magnetization, and spreading rates.

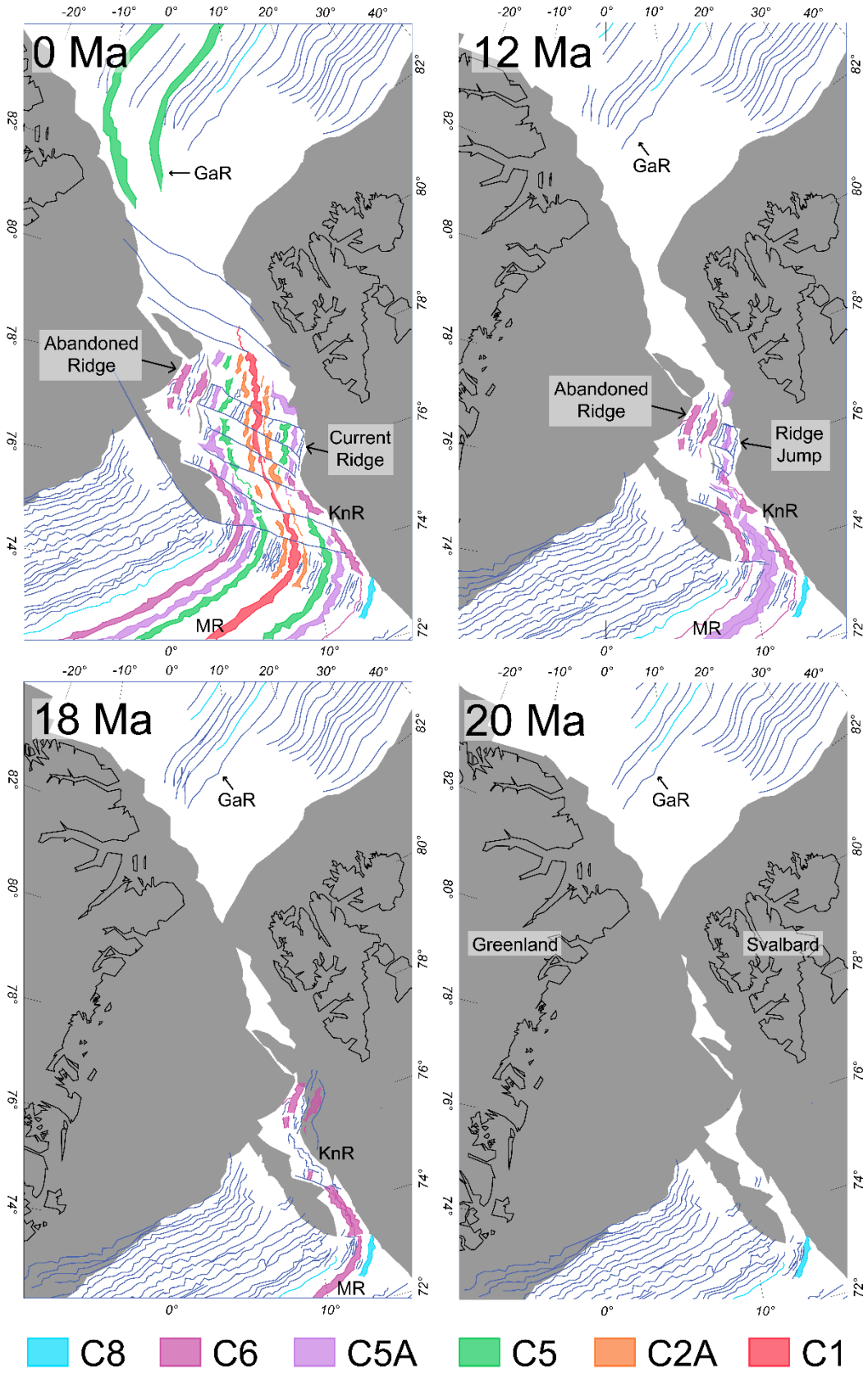

Figure 9. Reconstruction using the magnetic gridded data. The ridge in the Boreas Basin was abandoned at 18 Ma and jumped eastward towards Svalbard. Oceanic fracture zones, lineaments and magnetic isochrons are shown in turquoise (Dumais et al., accepted).

5.3 Magnetization compared to the High-resolution Bathymetry

A 3-D magnetization model of the KRAS-16 aeromagnetic dataset was calculated using an inversion method implemented in GM-SYS-3D (Geosoft, 2014; Parker & Huestis, 1974). The model was constrained by a Moho depth derived from seismic data (Funck et al., 2017), a sedimentary thickness (Engen et al., 2006) and bathymetric data (Olesen et al., 2010). The magnetization derived from the data represents the overall magnetization of the crust without differentiation of the lithology of the upper crust, lower crust, and numerous intrusions. It provides preliminary insights of the type of magnetization expected for the 2-D forward models.

The magnetization was correlated to the bathymetric highs and volcanic features of the ridge by superimposing the bathymetric contour lines (Figure 10). The bathymetric data were collected by Norwegian Petroleum Directorate in 2006-2010 (Zarayskaya, 2017).

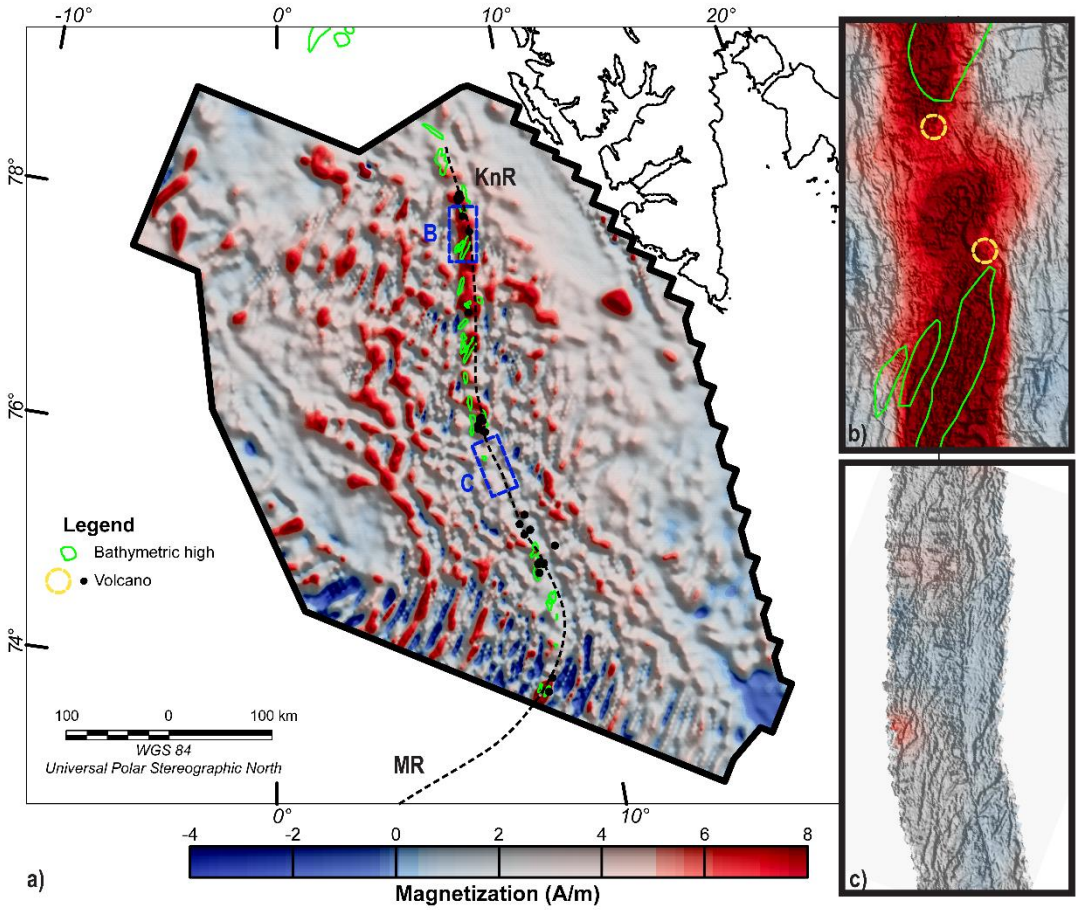

Figure 10. a) Calculated magnetization compared with the high-resolution bathymetric data (KnR: Knipovich Ridge, MR: Mohn's Ridge). b) Volcanic-like features and bathymetric highs of the seafloor within the rift valley correlate with magnetic highs. c) Whereas the absence of volcanic-like features correlates with less prominent magnetic highs or no magnetic highs (Dumais et al., submitted).

At the southern tip of the Knipovich Ridge, high-amplitude stripes of magnetization demark the transition from the Mohn's Ridge, alternating from -4 to +8 Am^{-1} associated with normal and reverse

remanent magnetization (Figure 10a). Following the Knipovich Ridge northward, at latitudes 74˚N-76˚N, the magnetization degrades to 0 to 4 A m^{-1} with rare occurrences of strong magnetization. A close analysis of the bathymetry within the rift valley draws a correlation between the presence of volcanoes and crater-shaped features, and bathymetric highs with high magnetization values (Figure 10b). Bathymetric highs and volcanoes generally occur in a rich magma supply setting. On the contrary, a low magma supply or an iron- and oxide-poor magma chamber would result in low magnetization, producing new oceanic crust poor in magnetite (Figure 10c). Seawater can percolate through fractures and change the thermal and chemical properties of the crust (Searle, 2013). Numerous lineaments and fracture zones are identified from the aeromagnetic dataset, which are partly linked with linear features from the bathymetric data. Fluid circulation leads to oxidation and degradation of the well-oriented magnetic grains, possibly changing the strong remanent magnetization into induced magnetization (Kent & Gee, 1996). At latitudes of 76˚N-78˚N, the central magnetic anomaly amplitude increases to reach values expected from a normal oriented remanence.

5.4 Crustal Thickness derived from Werner Deconvolution and the Curie Point Depth

The Curie point depth (Figure 11a) was derived from the aeromagnetic data with the Pycurious Python code (Mather & Delhaye, 2019) using the Bouligand et al. (2009) algorithm. The Curie point depth represents the isotherm of the Curie temperature of magnetite (580˚C). Above this temperature, the magnetite loses its magnetization. Therefore, the Curie point depth estimation should coincide with the bottom of the deepest causal magnetic source. The Curie point depth estimation is based on the aeromagnetic compilation of the high-resolution KRAS-16 dataset with the adjacent aeromagnetic datasets. The accuracy of the Curie point depth estimation from the magnetic data in the oceanic domain could be biased since the magnetization acquired during the seafloor spreading is not entirely random in all directions as expected by the methodology. However, given the observations from the magnetic data and the profiles modelling, the results appear reasonable and at least reliable to discretize oceanic and continental domains. In the Mohn's Ridge area, few kilometres south of KRAS-16 survey, an aeromagnetic profile is either missing or filtered for noise reduction and causes a linear trend with coarse resolution in the compilation. Since the Curie point depth calculation is sensitive to the frequency content of the magnetic data to derive the depth, shallow depths as expected in the oceanic domain cannot be resolved for this linear section (Figure 11a). The adjacent survey flown in the Greenland and Boreas basins, west of the KRAS-16 survey, also presents small discrepancies in the Curie point depth with deeper values (Figure 11a) likely caused by levelling issues of this adjacent survey.

The Werner deconvolution (Ku & Sharp, 1983; Phillips, 1997; Werner, 1955), an automated depth-to-source estimation method, was derived from the magnetic data. Using these empirical basement indicators, sensitive to susceptibility variations, and approximating the geological source to a simplified geometry of features such as contacts and dikes (Goussev & Peirce, 2010), the depth and morphology of the magnetic top basement and intrusions are estimated (Figure 11b). The Werner deconvolution solutions represent the depth to the top of the causal sources where specific clusters are observed. The resolution of the depth solutions depends on the resolution and accuracy of the magnetic data. The high-resolution KRAS-16 survey allowed reliable depth solutions, in contrary to

the aeromagnetic data in the adjacent areas and acquired with wider line-spacing, poor positioning and often filtered for noise reduction.

The Werner deconvolution solutions correlates with the oceanic domain interpreted form the magnetic data. Shallow sources of less than 5 km depth are observed in the oceanic domain (Figure 11b). Also, in the oceanic domain, the Curie point depth estimation indicates shallow depths varying between 5 and 7 km, where hotter temperature in the lithosphere are expected from the magma supply feeding the spreading ridge (Figure 11a). The oceanic crust is estimated to lie from less than 5 km (top) to 7 km (bottom) depth. The Curie point depth transitions to greater depths of 25 km in the continental domain, expressing a colder crust-mantle system. A large transition zone between the shallow oceanic basement (4-6 km) and the deep continental basement (25-30 km) is observed along the west boundary of the KRAS-16 survey. This section correlates with deeper Werner deconvolution solutions resolving deeper intrusions or a deeper top basement suggesting a thick sedimentary cover (Figure 11b). Thus, the top of the magnetic sources is expected at larger depth than 7 km and the bottom layer at 12 km+/-2 km depth.

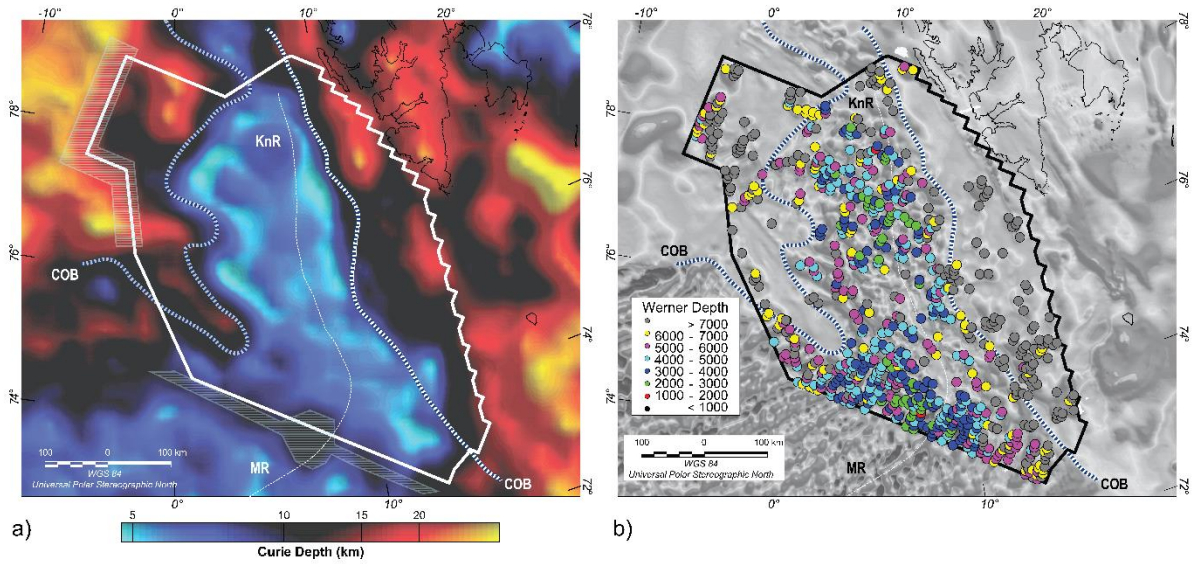

Figure 11. a) Curie point depth representing the bottom of the causal magnetic source calculated from the aeromagnetic compilation. The shallowest depth area agrees with the COB depicted from the magnetic data and constrains the oceanic domain. The grey hatched zone is the location where the Curie point depth is assumed erroneous due to poorer data quality. b) Werner deconvolution solutions derived from the aeromagnetic data representing the top of the causal magnetic source. Shallower depth solutions are observed in the oceanic domain (KnR: Knipovich Ridge, MR: Mohn's Ridge, COB: Continent-ocean boundary) (Dumais et al., submitted).

5.5 2-D Forward Modelling

GM-SYS-2D has been used to calculate the forward models of the studied profiles (Geosoft, 2006). The magnetic compilation and a compilation of publicly available gravity data were used for the modelling. The gravity data (Figure 12) used for latitudes below 80°N is the global marine gravity model (Sandwell et al., 2014). Above 80°N, the gravity data compilation relies on the Arctic Gravity Project (ArcGP) data compilation (Kenyon et al., 2008).

The models were constrained by available seismic and EM data. The Werner deconvolution provided a certain degree of constraints to map the top of the crustal basement and magmatic intrusions. Published horizon interpretation (Table 1) derived from OBS crustal seismic were applied as

structural constraints. Profile locations are shown on Fig. 1 and all profiles have been interpreted for the Moho, top crustal basement, and sedimentary layers in accordance with the seismic velocities.

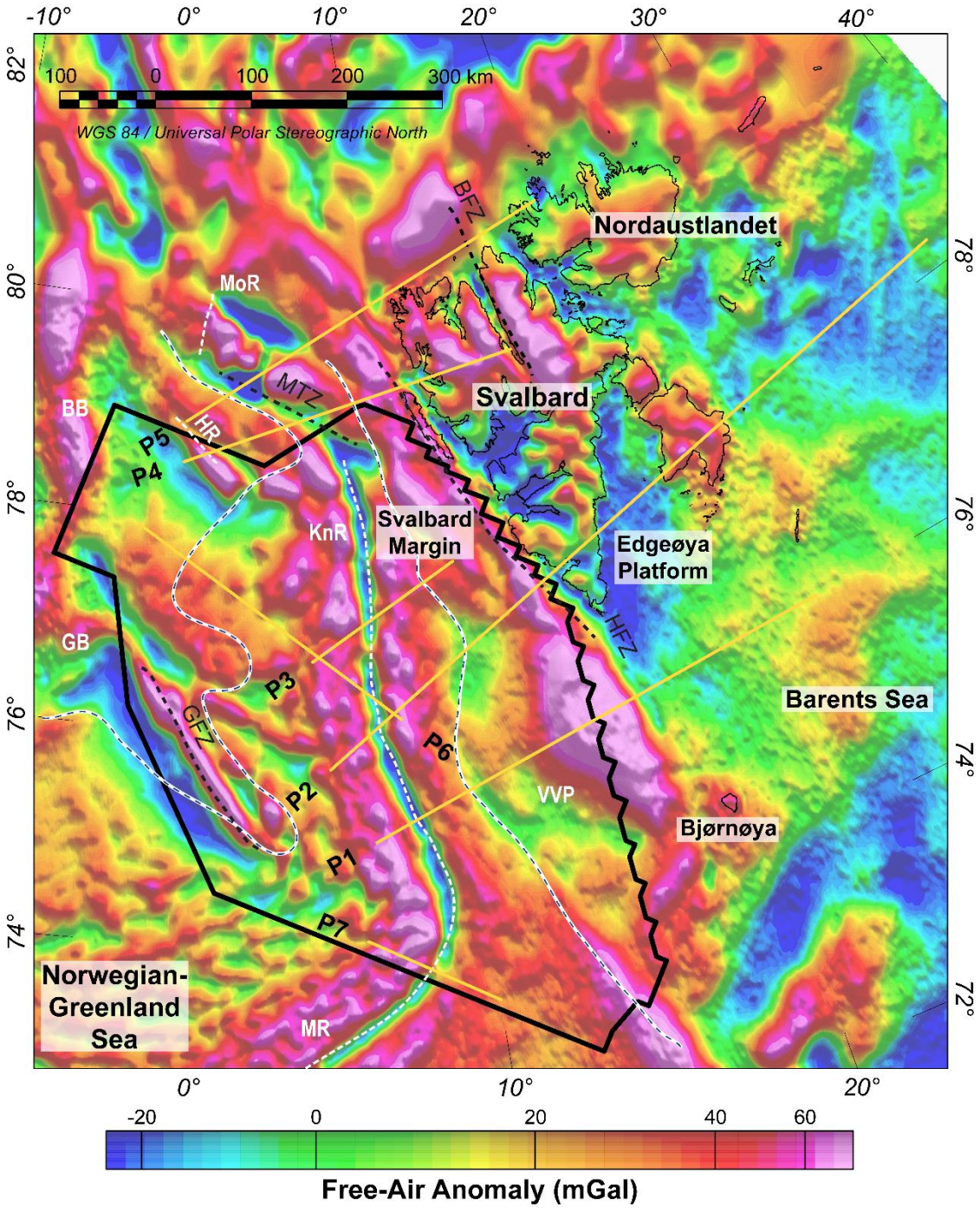

Figure 12. Free-air gravity anomaly maps of the area. (COB: blue dashed line, KRAS-16 boundary: black, 2-D profiles: yellow, lineaments map from the magnetic data: white: BB: Boreas Basin, BFZ: Billefjorden Fault Zone, GB: Greenland Basin, GFZ: Greenland Fracture Zone, HFZ: Hornsund Fault Zone, HR: Hovgaard Ridge, KnR: Knipovich Ridge, MR: Mohn's Ridge, MoR: Molloy Ridge, MTZ: Molloy Transform Zone, VVP: Vestbakken Volcanic Province) (modified after Dumais et al (submitted)).

Table 1. Description and reference of the 2-D modelling constrains. The location of the profiles is displayed in Figure 12.

Profile	Lines	Characteristics	References
1	Barents 98 Line 3W & E	Seismic	(Breivik et al., 2003) (Breivik et al., 2005)
2	Barents 98 Line 8 & 10, Hoersted'05	Seismic	(Ljones et al., 2004) (Breivik et al., 2005) (Czuba et al., 2008) (Grad & Majorowicz, 2020)
3	Barents 98 Line 9	Seismic	(Ritzmann et al., 2002)
4	AWI 99400	Seismic	(Ritzmann et al., 2004)
5	AWI 99200	Seismic	(Czuba et al., 2005)
6	AWI 20090200	Seismic	(Hermann & Jokat, 2013)
7	-	CSEM / MT	(Johansen et al., 2019) (Lim et al., submitted)

5.5.1 Profile 1

This profile crosses the ridge and ends in the Barents Sea, south of Svalbard. It presents a large gravity anomaly (Figure 13) which used to estimate the COB location in earlier studies, e.g. Breivik et al. (1999). The magnetic anomaly striped pattern demarks that the COB (Dumais et al., accepted) is located about 160 km farther west. This magnetic description of the COB is used for all models and data analysis of this current study. The central magnetic isochron C1 is amagmatic, with no clear magnetic signal, and modelled with low remanent magnetization. Intrusions or volcanic mounds in the Vestbakken Volcanic Province could explain the magnetic signature between the COB and the Hornsund Fault Zone. This 200-km section between the COB and the Hornsund Fault Zone showing no clear striped magnetic pattern is defined as a transition domain between the continental and the steady state oceanic crust domains. One large intrusion is modelled at the boundary between the transition and continental domain. The Hornsund Fault Zone is also denoted with a shallow narrow elongated intrusion due to the high frequency of the related magnetic anomaly. The depth of the bottom of this causal body cannot be estimated from the modelling, but the small response on the gravity signal suggests a small body in volume. East of the Hornsund Fault Zone, corresponding to a magnetic high, several intermediate magnetic anomalies are found on the Svalbard margin. These anomalies are modelled with several continental crustal layers superposed at an angle and with varying susceptibilities that are possibly related to old Caledonian nappes. There is no indication on the seismic data of a basement change in the lithology which agrees with the small density variation between the crustal layers.

A good correlation between the observed and calculated gravity anomalies requires a variation of the crustal and mantle densities. The upper crust in the oceanic domain consists of basalt with densities of 2,700-2,750 kg m^{-3} while the gabbro of the lower crust has a density of 2,900 kg m^{-3}. Densities in the transition domain defined in this study are 2900 kg m^{-3} and does not support a clear delimitation between the upper and lower crust which is consistent with the velocity observed along the seismic transect (Breivik et al., 2003; Breivik & Mjelde, 2001a, 2001b). The continental crust has densities of 2,900-2,990 kg m^{-3} overlain by felsic-granite rocks with density of 2,600-2,750 kg m^{-3} embedded by two sills imaged from the seismic data (Breivik & Mjelde, 2001b). The prominent

gravity high appearing in the middle of the profile (Figure 13) is caused by the bathymetry and not by a variation in the properties (density or thickness) of the crust or mantle. A gradual density variation from a thermal mantle was attempted as suggested by Breivik et al. (2003) for the continental section of the profile but could not explain the gravity for the full profile including both continental and oceanic section. The gravity did, however, require a density variation in the mantle. This was achieved with a lower density solely below the oceanic crust, suggesting that the variation of temperature in the mantle is local and does not require thermal variation over a long distance towards the transition or continental domain.

5.5.2 Profile 2

Profile 2 (Figure 14) crosses the Knipovich Ridge axis, the Svalbard Margin, Spitsbergen and terminates on the Edgeøya Platform. The COB depicted from the magnetic striped anomalies correlates with the gradual change in the velocity of the seismic interpretation in the upper crust from about 4.5-5.0 km s^{-1} to 5.5-6.0 km s^{-1} (Breivik & Mjelde, 2001a). The seismic interpretation of Profile 6 intersecting at point P6 on Figure 14 observed a mantle-crust interface at 6 km depth (Hermann & Jokat, 2013) instead of 9 km (Grad & Majorowicz, 2020). The present gravity model requires a thinner crust with a Moho 2 km higher than the Moho derived from the seismic interpretation for the oceanic and transition domain. The transition domain is defined between the COB and the Hornsund Fault Zone. The latter corresponds to a magnetic anomaly high. Densities in the transition domain are 2800-2970 kg m^{-3} consistent with the seismic velocities for both the upper and lower crusts (Breivik & Mjelde, 2001a, 2001b; Grad & Majorowicz, 2020). Several magnetic anomalies are modelled with higher susceptibilities representative of dikes in the transition domain. The mantle density also increases from the oceanic to the transition and continental domains. East of the Hornsund Fault Zone, the crustal properties change with higher densities and susceptibilities. The crust modelled is thicker (30 km), apparent to a continental crust. Intrusions are modelled on the Edgeøya Platform where sills and dikes are expected (Minakov et al., 2012). However, the current resolution of the magnetic data does not allow us to resolve the depth and volume of these magnetized bodies. Two high density bodies are modelled in the lower crust agreeing with the high velocity bodies interpreted with the seismic data which were correlated with the lithosphere-asthenosphere boundary (LAB) uplift (Grad & Majorowicz, 2020).

5.5.3 Profile 3

This profile crosses the Knipovich Ridge axis to the Svalbard Margin (Figure 15). The profile is located between two magmatic segments in the rift valley (Figure 12). The COB demarked by the striped magnetic anomaly correlates with the gradual change in the velocity of the seismic interpretation in the upper crust (Breivik & Mjelde, 2001a). The lower crust below the Knipovich Ridge requires a lower density (2750 kg m^{-3}) than the surroundings (Figure 15). The gravity model also requires a lower mantle density in the oceanic domain (3280 kg m^{-3}). The profile was compared to Profile P6 which was interpreted with a thinner crust. The Moho was raised up by 2 km west of the rift valley improving the agreement between the modelled and observed gravity profile. This also reduces the crustal thickness difference at the intersection between Profiles P3 and P6.

5.5.4 Profile 4

This profile (Figure 16) starts at the Hovgaard Ridge extending through the Molloy Transform Zone and terminates onshore Svalbard (Figure 12). The crust below the Molloy Transform Zone was modelled with a density of 2800 kg m^{-3} that is lower than the values beneath the Knipovich Ridge

(2900 kg m^{-3}). Two magmatic bodies are modelled between the Molloy Transform Zone and Spitsbergen. In that area, east of the Molloy Transform, the observed magnetic profile has higher values than the modelled magnetic profile. This section is challenging to interpret due to the poor data quality. It could be modelled with remanent magnetization diagnostic of an oceanic crust; however, no magnetic striped pattern is observed in the gridded data (Figure 8). Local serpentinization of exhumed mantle rocks could also explain the magnetic high.

The mantle density under the Molloy Transform Zone is reduced to 3270 kg m^{-3}, a value slightly lower than the interpretation under the Knipovih Ridge. A serpentinization process could explain the reduced density of the mantle required below the Molloy Transform Zone. Similar to Profiles 1 and 2, a thick continental crust with high density (2930-3000 kg m^{-3}) is modelled. The original seismic interpretation (Ritzmann et al., 2004) suggested a low velocity crust but the gravity modelling necessitates higher densities than expected. The continental section of the profile can be interpreted as compacted sediments of Devonian age (2730 kg m^{-3} and <0.0001 SI) on a basement of Precambrian age (2920-2950 kg m^{-3} and 0.03 SI).

5.5.5 Profile 5

Profile 5 (Figure 17) starts west of the Molloy Ridge, crosses north of Spitsbergen and ends offshore Nordaustlandet. The rift valley is not aligned with the highest section of the Moho. The magnetic striped pattern indicative of an oceanic crust is not observed on the gridded magnetic data (Figure 8). The data accuracy and resolution could not allow us to resolve magnetic isochrons and to determine the spreading of the Molloy Ridge. Therefore, the COB is difficult to interpret from the magnetic data as the profile is located outside the high-resolution KRAS-16 survey. The Billefjorden Fault Zone is associated with a magnetic high as previously described by Skilbrei (1992). A large magmatic intrusion is modelled west of the rift valley. The thin lower crust between the Molloy Ridge and Spitsbergen is strongly magnetized (0.025 SI) with lower density than the lower crust interpreted beneath the Knipovich Ridge.

Similar to Profile 4, low crustal velocities (6.0-6.5 km s^{-1}) were interpreted on Profile 5 (Czuba et al., 2005). However, the gravity model requires higher densities (2900-2950 kg m^{-3}). Given the density and susceptibility comparable to Profile 4 (Figure 16), the continental domain can be interpreted as Devonian compacted sediments on a Precambrian basement. The gravity interpretation of the mantle correlates with Profile P4 requiring low density (3270 kg m^{-3}) beneath the Molloy Ridge and higher densities (3330 kg m^{-3}) farther away. The gravity model slightly disagrees with the observed data at the Molloy Ridge and at the shallowest point of the Moho. The Molloy Ridge requires an increase of density or a thinner crust while the shallowest point of the mantle requires a decrease of density or a thicker crust. Modifying the geometry of the crust would move the shallowest point of the mantle towards the Molloy Ridge improving the alignment between the rift valley and the shallow Moho.

5.5.6 Profile 6

This profile runs from the Boreas Basin and crosses the Knipovich Ridge (Figure 18). It also intersects Profiles 2 and 3 at point P2 and P3. It is mostly located in the oceanic domain where the striped magnetic signal is found. A small portion is located in the transition domain. An extinct oceanic ridge has been determined from the KRAS-16 dataset (Dumais et al., accepted). The magnetization values are generally low, and the striped pattern is not clear between the current Knipovich Ridge and the

extinct ridge (Figure 18). At this location, the gridded magnetic data show a fracture zone or lineament underlying the seismic profile consistent with the lack of a magnetic striped pattern. However, the magnetic striped pattern is clearly recognized a few kilometres away from the profile. The crustal thickness and densities below the extinct ridge and the current spreading ridge are similar. On the western half of the extinct ridge, the crustal density increases. The crustal thickness increases west of the extinct ridge. The mantle density is lower below the present-day spreading ridge like profiles 1, 2 and 3. Along profiles 2 and 3, the crustal thickness has been adjusted to Profile 6 as the crustal thickness of P6 is more representative of a slow-spreading system. For profiles 2, 3 and 6, the resulting models with a thinner crust agree with the observed gravity data. The mantle density under the extinct ridge is higher than the mantle density under the present-day ridge, perhaps indicative of a colder mantle. The mantle density increases west of the abandoned ridge but remains lower than the transition mantle densities modelled east of the Knipovich Ridge for profiles P1, P2 and P3.

5.5.7 Profile 7

Profile 7 (Figure 19) is located on the oceanic domain located at the junction between the Knipovich and Mohn's ridges. The magnetic interpretation was described by Lim et al. (submitted). The central anomaly presents a small depression in the middle of the anomaly caused by the presence of two mounts in the rift valley. The eastern lobe of the central anomaly is slightly higher than the western lobe. The basalt layer is about 1 km in thickness with a heterogeneous magnetization. The magnetization values have slightly changed from Lim et al. (submitted) interpretation due to adjustment between the profiled data and the merged magnetic compilation, but the geometry remains unchanged. The mantle density directly under the rift valley are reduced as suggested by the mantle temperature gradient (Johansen et al., 2019). The disagreement between the modelled and observed gravity profiles is explained by the coarse resolution of the gravity data compared to the resolution and accuracy of the CSEM interpretation. The geometry of the CSEM interpretation requires smaller wavelength not recorded in the gravity data. However, the gravity model requires a lateral density variation of the mantle as suggested by the MT thermal interpretation. This local density variation indicates the narrow nature of the thermal model. However, higher resolution gravity data is necessary to reconstruct the density gradient below the Knipovich Ridge.

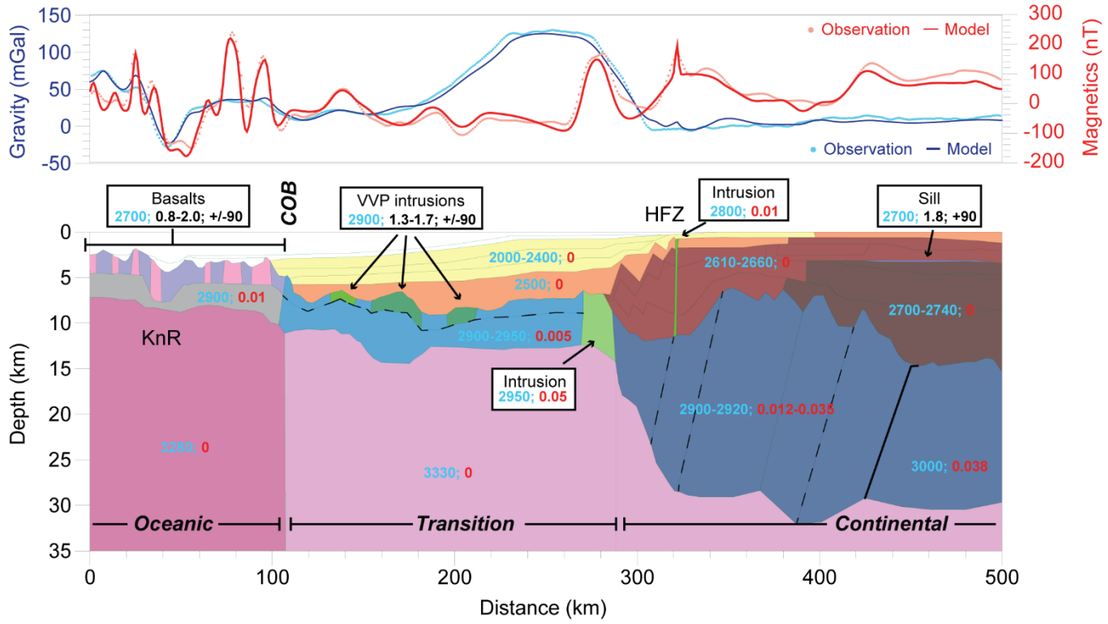

Figure 13. Profile 1 - 2-D profile with the modelled and observed data for gravity and densities (kg m^{-3}, blue), and for the magnetic, susceptibility (SI, red) and magnetization (A m^{-1}; inclination ˚) are shown. (KnR: Knipovich Ridge, HFZ: Hornsund Fault Zone).

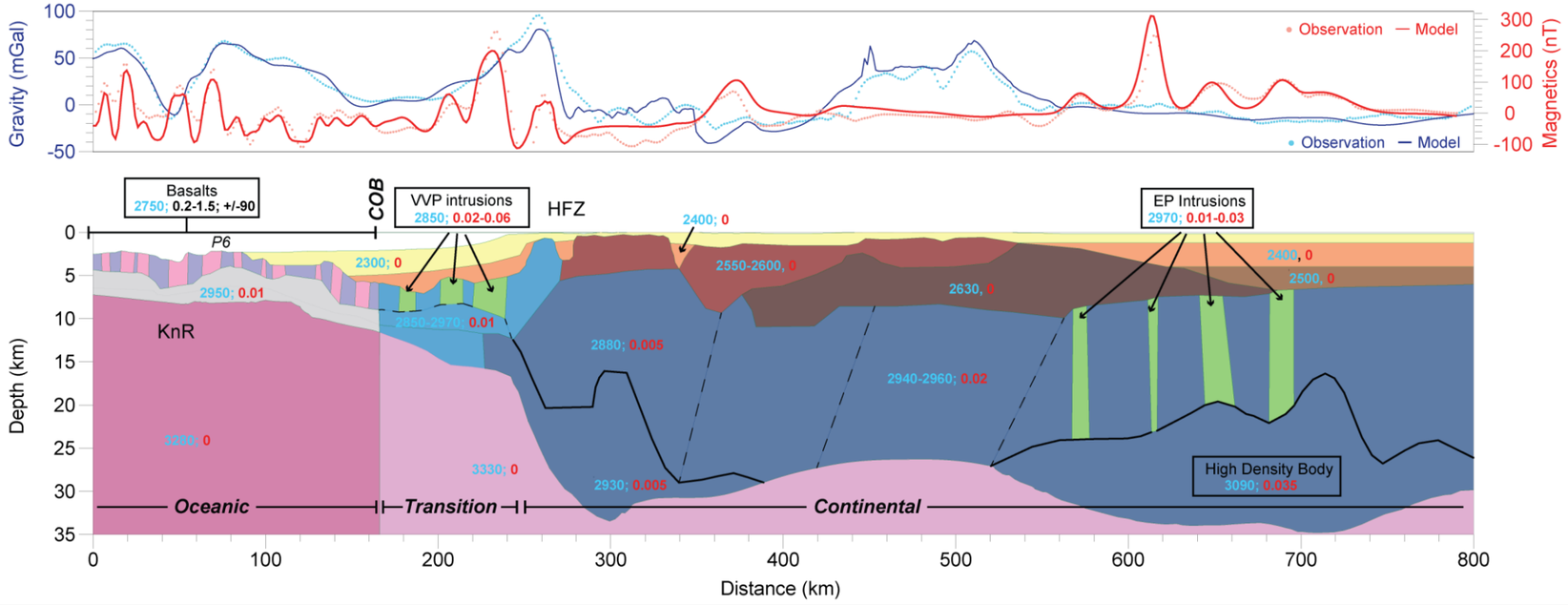

Figure 14. Profile 2 - 2-D profile with the modelled and observed data for gravity and densities (kg m^{-3}, blue), and for the magnetic, susceptibility (SI, red) and magnetization (A m^{-1}; inclination ˚) are shown. (EP: Edgeøya Platform, KnR: Knipovich Ridge, HFZ: Hornsund Fault Zone, P6: Profile 6).

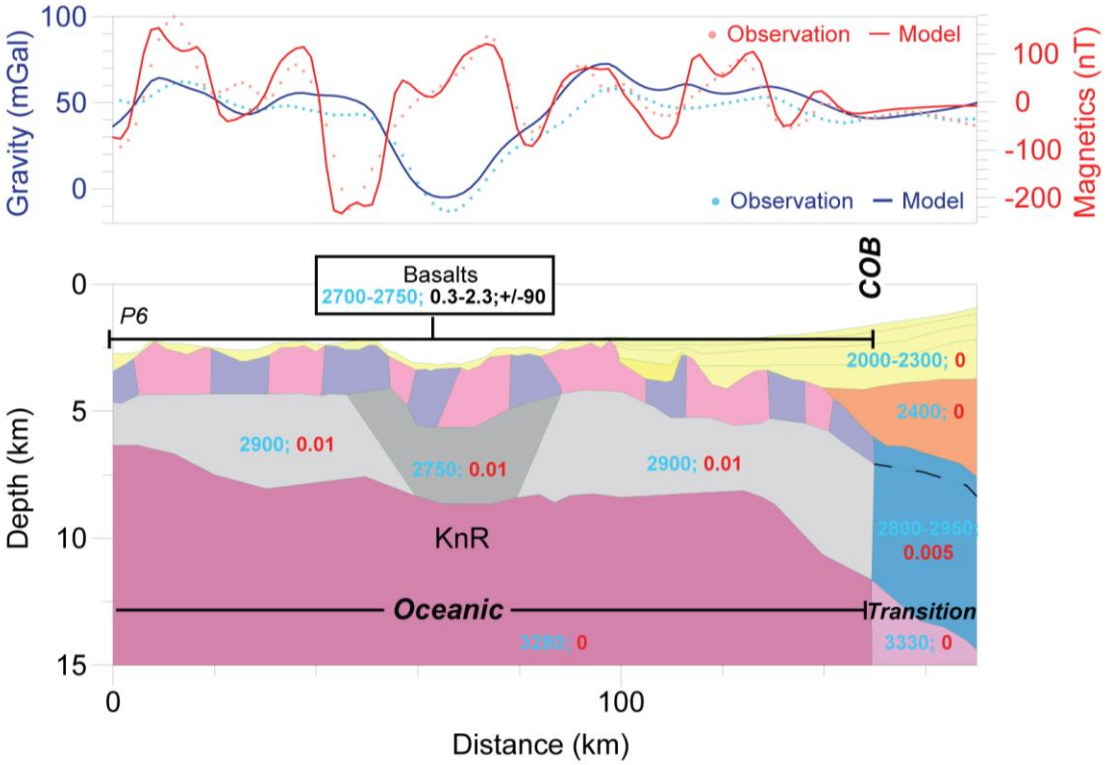

Figure 15. Profile 3 - 2-D profile with the modelled and observed data for gravity and densities (kg m^{-3}, blue), and for the magnetic, susceptibility (SI, red) and magnetization (A m^{-1}; inclination ˚) are shown. (KnR: Knipovich Ridge, P6: Profile 6).

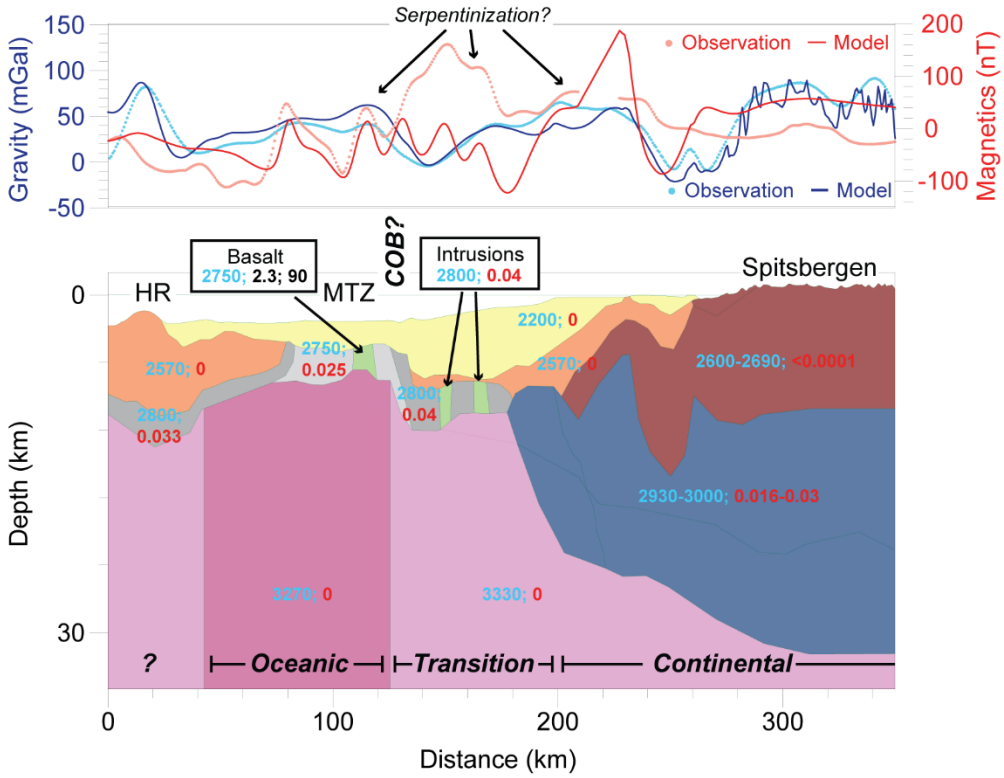

Figure 16. Profile 4 - 2-D profile with the modelled and observed data for gravity and densities (kg m^{-3}, blue), and for the magnetic, susceptibility (SI, red) and magnetization (A m^{-1}; inclination ˚) are shown. (HR: Hovgaard Ridge, MTZ: Molloy Transform Zone).

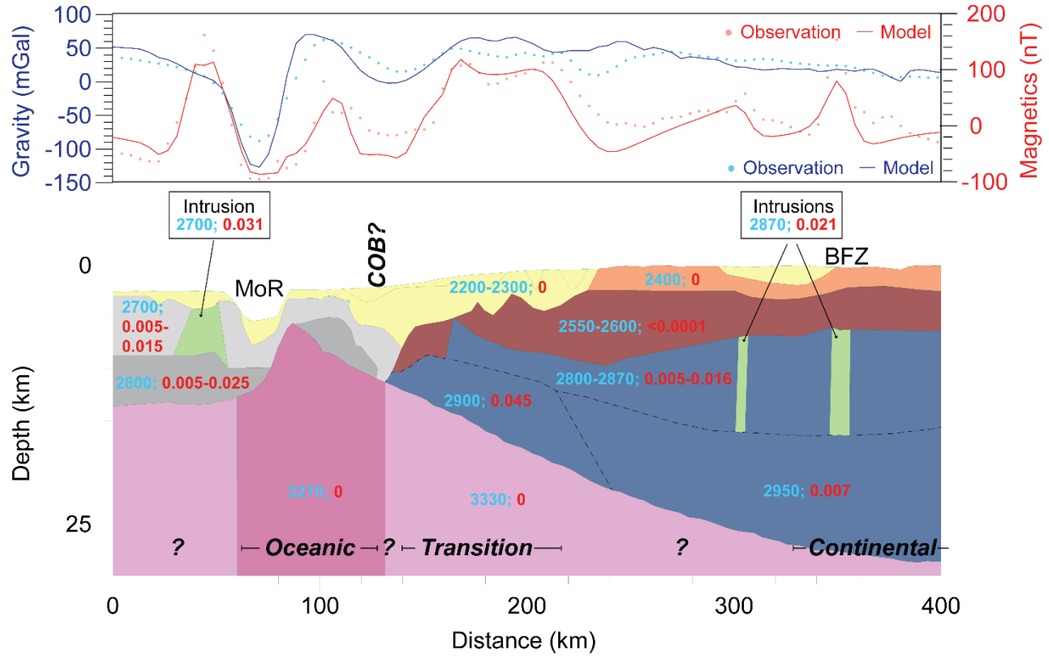

Figure 17. Profile 5 - 2-D profile with the modelled and observed data for gravity and densities (kg m^{-3}, blue), and for the magnetic, susceptibility (SI, red) and magnetization (A m^{-1}; inclination °) are shown. (MoR: Molloy Ridge, BFZ: Billefjorden Fault Zone).

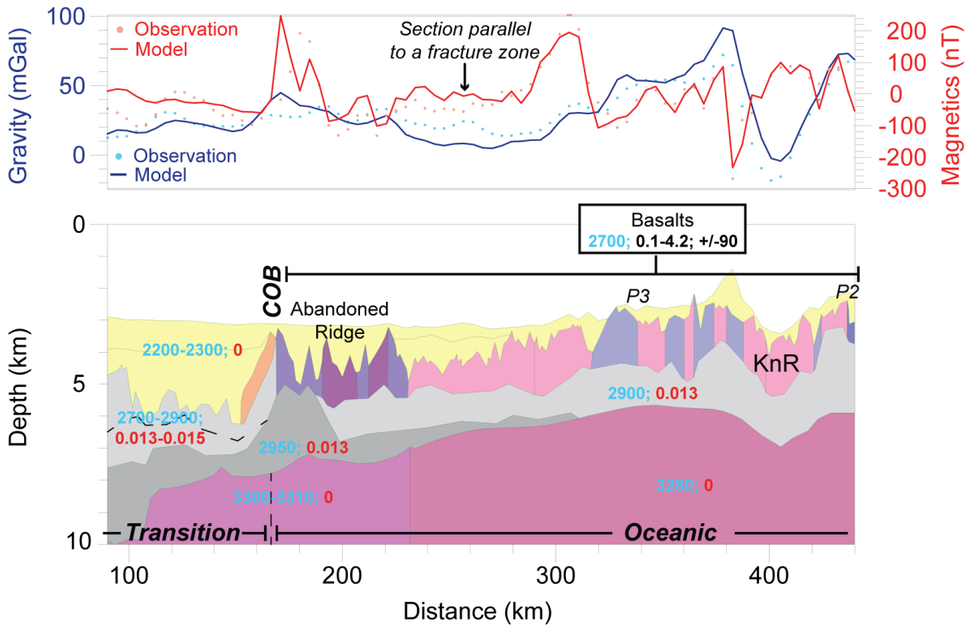

Figure 18. Profile 6 - 2-D profile with the modelled and observed data for gravity and densities (kg m^{-3}, blue), and for the magnetic, susceptibility (SI, red) and magnetization (A m^{-1}; inclination °) are shown. (KnR: Knipovich Ridge, P2: Profile 2, P3: Profile 3).

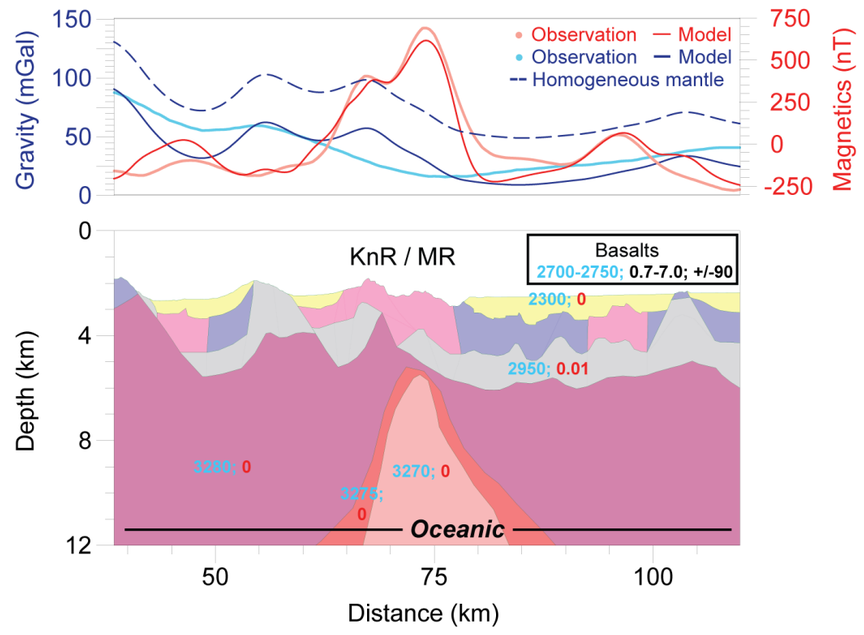

Figure 19. Profile 7 - 2-D profile with the modelled and observed data for gravity and densities (kg m^{-3}, blue), and for the magnetic, susceptibility (SI, red) and magnetization (A m^{-1}; inclination °) are shown. (KnR: Knipovich Ridge, MR: Mohn's Ridge).

The 2-D forward models are consistent with the COB interpretation from the aeromagnetic data. The profiles are put in a 3-D perspective in Figure 20.

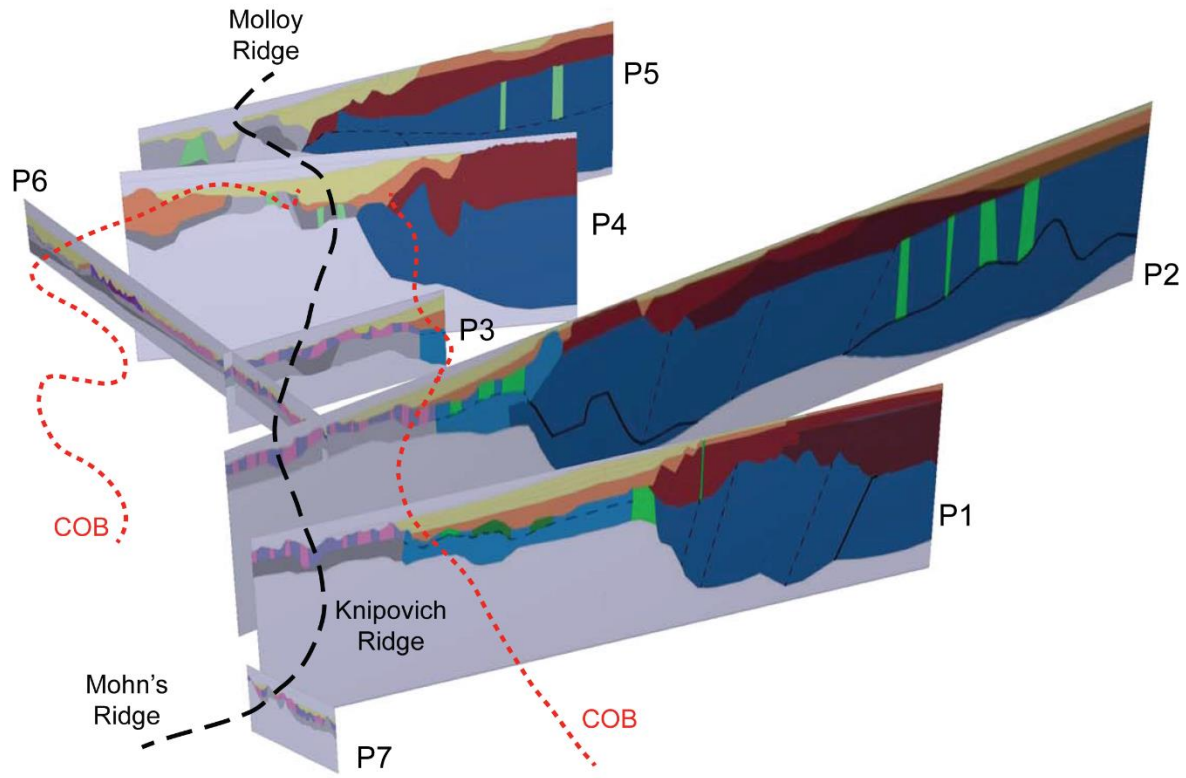

Figure 20. 3-D view of the 2-D forward models with the COB and the ridge superimposed.

6 Discussions

The interpretation results demark the COB greatly debated in the North Atlantic and Arctic Oceans and in the Fram Strait in particular (Breivik et al., 1999; Faleide et al., 2008; Gernigon et al., 2019; Voss & Jokat, 2007), and confirm the opening of the Knipovich Ridge initiated at 20 Ma (C6) where the first unambiguous magnetic anomaly appears. The Knipovich Ridge opening occurs obliquely to the Mohn's Ridge and developed after the opening of the Norwegian-Greenland Sea and the Eurasian Basin already initiated in the Early Eocene (Brozena et al., 2003) and the extinction of the Mid-Labrador Ridge at C13 (Gaina et al., 2009; Oakey & Chalmers, 2012; Suckro et al., 2013). This coincides with the opening of the Molloy Ridge (20 Ma, (Trulsvik et al., 2011)) and Kolbeinsey Ridge (C7-6, (Blischke et al., 2017; Schiffer et al., 2019)), and the Gakkel Ridge penetrating in the Fram Strait (C8-5, (Glebovsky et al., 2006)).

East of Knipovich Ridge, the new COB is closer to the ridge by up to 160 km compared to previous interpretations (Breivik et al., 1999). The oceanic crust, enclosed by magnetic isochrons C6, is relatively thin, up to 5 km (Johansen et al., 2019), and characterized by remanent magnetization from the presence of basalts. The crustal sections between magnetic isochrons C6 and the rifted margins, on either side of the Knipovich Ridge, are representative for a stretched crust with no apparent striped magnetic anomalies associated with an authentic oceanic crust. The presence of rounded, intermediate-size magnetic anomalies suggests magmatic intrusions occurring in this area.

The 3-D magnetization and 2-D forward interpretations delineated the crustal domains of the area. The oceanic and continental domains are derived from the crustal thickness and properties in terms of susceptibility, remanence, and density. A wide transition domain was also delineated between the oceanic and continental domains.

6.1 Oceanic Domain

The Oceanic domain, delimited by the COB ridge-ward, comprises striped magnetized anomalies. As observed in the 3-D magnetization model and the 2-D forward models, the rift valley of the ridge varies northward from almost none to high magnetization. The high magnetization areas correlate with the presence of volcanoes and the bathymetric highs in the rift valley of the Knipovich Ridge, suggesting the oceanic crust has different physical properties than at the southern latitudes of the Knipovich Ridge. Therefore, the mantle processes, the volume and composition of the magma chamber below the ridge and the cooling processes are expected to vary from south to north. An iron- or oxide-rich magma chamber at latitudes 76˚N-78˚N compared to the southern section of the Knipovich Ridge could explain the presence of volcanoes and higher magnetization (Figure 10b). Multiple fracture zones and the bend with the Mohn's Ridge may cause a fluid interaction with the basalt layers of the oceanic crust, de-magnetizing the basalts. Given the low magnetization at the lower latitudes (74˚N-76˚N), an amagmatic segment is proposed to explain the low magnetization.

The shallowest values of the Curie point depth estimation correlate with the COB independently of the magnetization intensity. The Curie point depth estimation is around 6 km below the sea-level in the oceanic domain and slowly increases landwards (Figure 11a). The Werner deconvolution resolves a shallow crustal basement in the oceanic domain with solution depths of 2-4 km below the sea-level, representing the basalt layer lying near the seafloor surface. At magnetic isochron C6, the solutions are at 5-6 km below the sea-level suggesting a thicker sediment layer. No Werner deconvolution solutions are found where the magnetization is positively low.

A lateral density variation was modelled for the mantle for all the 2-D forward profiles. Local decreased mantle densities are interpreted in the oceanic domain. Low mantle densities are also required under the extinct ridge identified on Profile 6 (Figure 18). The lowest mantle densities are found under the active rift valley in Profile 7 (Figure 19), the highest resolution profile which offers a unique view of the Knipovich Ridge thermal heat variation. However, the gravity data resolution does not allow to accurately model the density variation correlated to the thermal mantle variation. The 2-D forward model does not support an isostatic equilibrium thermal distribution but agrees with a thermal variation between the oceanic and continental domains as suggested by Breivik et al. (1999). The lateral variation is more discrete and narrowly concentrated under the oceanic domain.

6.2 Continental Domain

The continental domain lies roughly eastward from the Hornsund Fault Zone (Figures 12-14). This demarcation is seen on the 2-D forward models where the crust is thick, with densities of 2850-2950 kg m^{-3} and Moho depth of 30 km below the sea-level. The Curie depth (Figure 11a) also reaches a depth of 25-30 km depicting a colder crust compared to the oceanic domain. The free-air and magnetic maps contain low-frequency anomalies, associated with a deep basement (Figure 8 and Figure 12). Intermediate anomalies (Figure 8) are likely associated with magmatic intrusions such as dikes or sills. Their emplacement and depth are estimated in the 2-D forward models (Figures 12-14). A high magnetic anomaly is found along the Hornsund Fault Zone where the basement rises to the

seafloor on Profile 2 (Figure 14). On Profile 1 (Figure 13), the magnetic anomaly is pronounced (Figure 8) and requires a magmatic intrusion (0.01 SI) along the Hornsund Fault Zone. Dikes and sills are modelled on the Edgeøya Platform expressing a largely intruded basement. On Profile 5 (Figure 17), the basement is more magnetized between the Molloy Ridge and Spitsbergen and an intrusion is associated with Billefjorden Fault Zone.

On Profiles 1 and 2, the basement susceptibility and density gradually vary across the continental domain. These variations can be associated with possible Caledonian nappes gradually extending on the margin. Profiles 4 and 5 present a different basement configuration with higher susceptibility and density in the lower crust modelled at the demarcation between the transition and the continental domains.

6.3 Transitional Domain

The oceanic and continental domains have a clear signature on the gravity and magnetic maps and are well tested and illustrated by the 2-D forward models. The oceanic and continental domains are separated by a distinct transition domain that extends by tens of kilometres (Figure 8 and Figure 21). The Curie depth allows to estimate the extent of the transition domain on both sides of the ridge (Figure 11a) where the Curie point depth migrates from shallow (6 km below sea-level) to deep (25-20 km below sea-level). This transition is also marked by a gradual thickening of the crust and a lack of magnetic striped pattern (Figures 12-18). The transition domain shares higher mantle densities compared to the adjacent oceanic domain. Similar mantle densities are also expected in the continental domain (Figures 12-18). The transition domain is wider at latitude 76°N and slowly narrows until latitude 80°N where it reaches its minimal extent on the eastern margin. On the western margin, the transition domain comprises the East-Greenland Ridge and a large portion of the Boreas Basin.

Sparse magnetized bodies in the transition domain have an estimated depth of 6-7 km below the sea-level or deeper which locate them in the upper crustal layer on the eastern margin while they can be shallower (5-7 km below sea-level) on the western margin according to the Werner deconvolution (Figure 11b). Intrusions are more numerous in the south-east margin, near the Vestbakken Volcanic Province. At that latitude, the conjugate margin is demarked by the prominent East-Greenland Ridge and a long amagmatic segment of the Knipovich Ridge characterized with low magnetization. On the north-east margin of the Knipovich Ridge, few major intrusions are found, but more prominent intrusions are located at the same latitude on the western margin in the Boreas Basin.

The Knipovich Ridge initiated in a transtensional system, where the plate was sliding along the Hornsund Fault Zone causing pull-apart basin infilling with thick sediments. Three scenarios could provide explanation to the observations in the transition zone.

1. The transition domain could comprise an oceanic crust buried under a thick sediment layer. One may consider the numerous intrusions found on profiles 1 and 2 in the transition domain have similar magnetic response to the oceanic magnetic isochrons. However, those intrusions have a rounded shape in the magnetic map and are not linear as commonly expected for oceanic spreading anomalies. Moreover, no corresponding anomalies are found on the conjugate margin. The crustal

properties of the transition domain are apparent to the continental crust with higher densities in the transition domain on profiles 1, 2 and 3 (Figure 12-14).

2. Alternatively, the transition domain could be formed by mantle exhumation and serpentinization. During the rifting before the spreading of the ridge, the continental crust was extended and thinned while the rift was filled with sediments. Significant hyperextension could have initiated the progressive exhumation and denudation as of the exhumed mantle as acknowledged on the Iberian margin (Pérez-Gussinyé et al., 2001; Sutra & Manatschal, 2012; Whitmarsh et al., 1993).This is consistent with the crustal structure interpreted by the seismic profiles and the crustal properties apparent in the continental domain. The crust could have been highly intruded during the mantle exhumation. The high-density lower crust could represent exhumed serpentinized mantle (Minshull, 2009). However, the Moho is well defined by the refraction waves whereas it is usually unclear in a heavily serpentinized mantle setting.

3. Finally, the transition domain could represent an exhumed lower continental crust as observed in many hyperextended rift systems (Clerc et al., 2015). During the rifting but before the spreading initiation at C6, the intruded continental lower crust could have gradually migrated and exhumed (Figure 21) towards the proto-oceanic domain. A pre-existing thick and low-viscosity lower continental crust caused by the Eurekan orogeny could explain a lateral flow of the ductile lower crust. Given the seafloor spreading initiation at C6 (20 Ma), the Eurekan deformation occurred prior to the ridge spreading (Piepjohn et al., 2016). The Eurekan deformation could have thickened and softened the crust. A rapid collapse and rifting could have led to a lateral escape of the lower continental material. This scenario is consistent with the crustal and mantle properties interpreted in the 2-D forward models.

The third scenario is favoured given the tectonic setting in the Fram Strait before the spreading initiation of the Knipovich Ridge. The 2-D forward models illustrate the evolution of the spreading ridge from the continental to the oceanic crust. The structure and composition of the crust, and the properties of the mantle were extracted from the profiles across the Knipovich Ridge. However, the modelling used seismic constraints from independent interpretations and not directly from digital seismic data. This remains an inherent uncertainty to the geometries and physical properties derived from the potential field modelling in this study. Nevertheless, the gravity and magnetic interpretation indicates that the Fram Strait has opened in a complex setting causing the asymmetric and heterogeneous oceanic and transition domains.

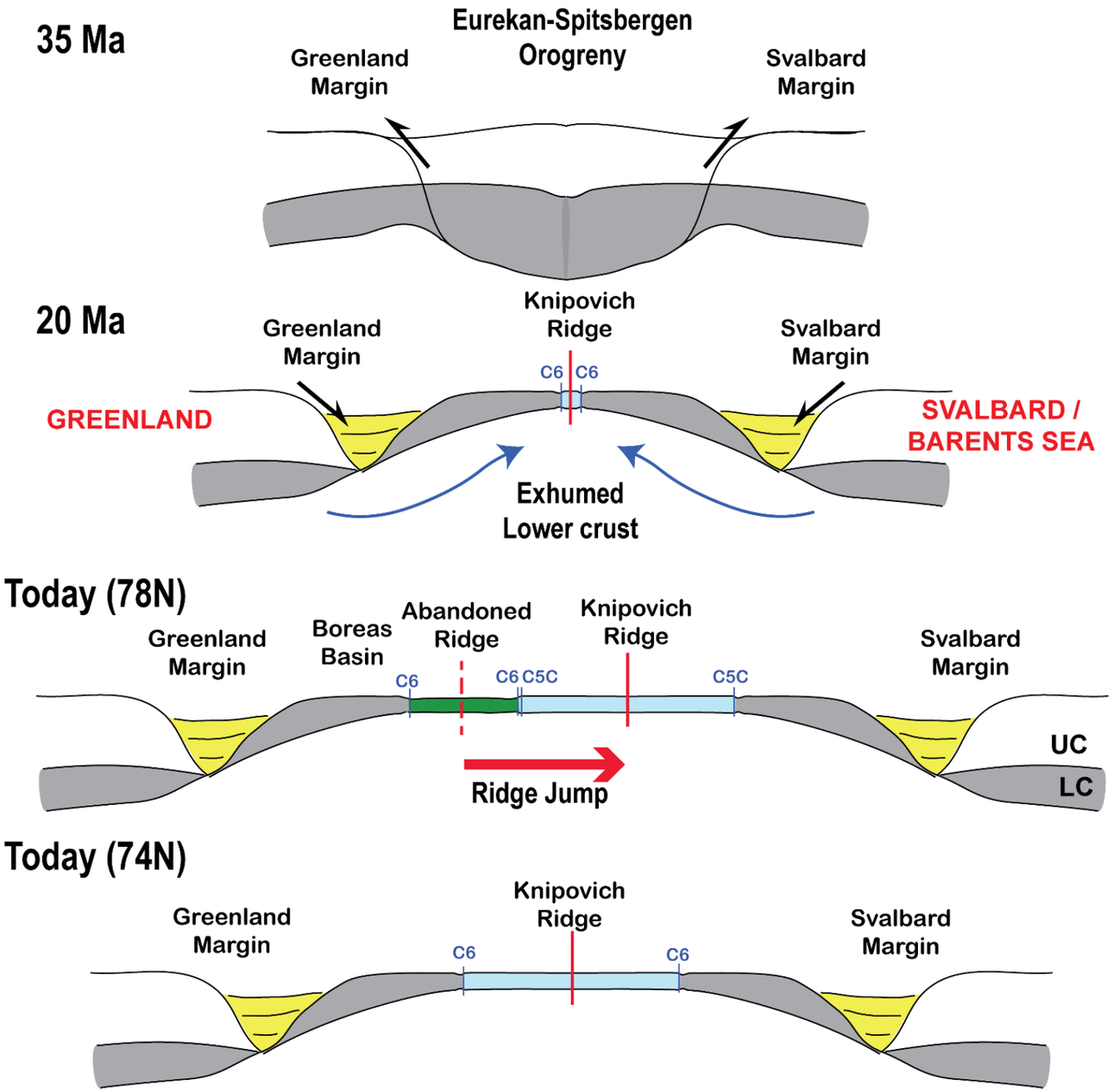

Chron	Age (Ma)	Event	References
	55-35	Eurekan-Spitsbergen orogeny	
13	36	Labrador ridge cessation	Engen et al., 2008 Oakey & Chalmers, 2012 Suckro et al., 2013
	35	VVP magnetic intrusion	Faleide at al., 2008
8-5		GaR opening in the Fram Strait	Glebovsky et al. 2006
7-6	24	KoR opening	Blischke et al., 2017
6	20	KnR opening	This study
5C-5E	18	Ridge migration to the east	This study
	10-15	Svalbard margin formation	
5	10	Iron-, oxygen- poor magma chamber(south section of KnR)	This study
	5	VVP magnetic intrusion	Mørk & Duncan, 1993
	0-20	Svalbard undergoes erosion	

Figure 21. Schematic profiles of the opening of the Knipovich Ridge. North (78˚N): the ridge in the Boreas Basin is abandoned (or extinct) and jumped eastward towards Svalbard to become present-day Knipovich Ridge. South (74˚N), the ridge has continuously opened since breakup around 20 Ma. UC: Upper crust, LC: Lower crust, VVP: Vestbakken Volcanic Province, GaR: Gakkel Ridge, KoR: Kolbeinsey Ridge, KnR: Knipovich Ridge (Dumais et al., accepted).

7 Conclusions

The present study aims at describing and modelling the crustal and mantle heterogeneities along the Knipovich Ridge and its surrounding margins using 2-D and 3-D modelling methods. The new KRAS-16 aeromagnetic data shed light on the development and crustal deformation to this rare configuration of two segments of the NE Atlantic spreading system. Aeromagnetic data from previous works were compiled to provide a global overview of the transition to the continental domain. The gravity compilation, the EM interpretation and the seismic interpretation provided indications and constraints to the gravity and magnetic interpretation.

1. Despite the 90-degree bend between the Mohn's and the Knipovich ridges, the opening at the southern section of the Knipovich Ridge is continuous from the Mohn's Ridge, underlining the eminent transtensional plate motion in the high Arctic.
2. The oceanic crust is clearly demarked by the striped magnetic pattern and its location confirmed by the 2-D forward models. The continent-ocean boundary (COB) is derived from this interpretation and confirmed by the modelling. The Knipovich Ridge initiated at C6 (20 Ma) and suggests the presence of numerous oceanic fracture zones and a broad continent-ocean transition interpreted as exhumed lower continental material.
3. The initiation of the spreading is delineated by the magnetic isochron C6 (20 Ma). A ridge jump is inferred in the Fram Strait around magnetic isochron C5E (18 Ma) and an extinct ridge is modelled in the Boreas Basin. The presence of this failed oceanic basin east of the Boreas Basin with a thin crust finally explains the peculiar strong asymmetry of the spreading system.
4. The Knipovich Ridge spreading initiated shortly after of the Kolbeinsey Ridge initiation and Gakkel Ridge prolongation. It may indicate a common link of mid-Atlantic ridge segments allowing a synchronous initiation of breakup at several locations of the North Atlantic-Arctic realm.
5. The magnetization in the oceanic domain is linked to the presence of volcanoes and bathymetric highs in the rift valley. Iron- and oxide-rich segments are identified along the rift valley.
6. The delineation of several lineaments and the bend configuration of the southern segment of the Knipovich Ridge is associated with a variation in the magnetization and settings along the Knipovich Ridge. It possibly controls the spreading settings and fluid circulation.
7. Mantle heterogeneities occur with an east-west lateral density variation and indicate a transition from a hotter mantle in the oceanic domain to a colder mantle underneath the older continental crust.
8. We favour the presence of a wide transition lithospheric domain comprising an exhumed lower crust or mantle. Compared to previous interpretation, we extend the Norwegian continental domain by up to 160 km farther west in the study area.

8 Acknowledgements

We are grateful to the European Plate Observing System – Norway, the Geological Survey of Norway, and the Norwegian Petroleum Directorate to finance the project. We are thankful to Novatem, Inc. for the data acquisition and preliminary data processing.

9 References

Blischke, A., Gaina, C., Hopper, J. R., Péron-Pinvidic, G., Brandsdóttir, B., Guarnieri, P., et al. (2017). The Jan Mayen microcontinent: an update of its architecture, structural development and role during the transition from the Ægir Ridge to the mid-oceanic Kolbeinsey Ridge. *Geological Society, London, Special Publications*, *447*(1), 299-337. https://doi.org/10.1144/sp447.5

Bouligand, C., Glen, J. M. G., & Blakely, R. J. (2009). Mapping Curie temperature depth in the western United States with a fractal model for crustal magnetization. *Journal of Geophysical Research: Solid Earth*, *114*(B11). https://doi.org/10.1029/2009jb006494

Breivik, A., Mjelde, R., Grogan, P., Shimamura, H., Murai, Y., & Nishimura, Y. (2003). Crustal structure and transform margin development south of Svalbard based on ocean bottom seismometer data. *Tectonophysics*, *369*, 37-70.

Breivik, A., Mjelde, R., Grogan, P., Shimamura, H., Murai, Y., & Nishimura, Y. (2005). Caledonide development offshore–onshore Svalbard based on ocean bottom seismometer, conventional seismic, and potential field data. *Tectonophysics*, *401*, 79-117.

Breivik, A. J., & Mjelde, R. (2001a). Obs-98 survey: Final report oceanic profiles. *Report*, *Univ. of Bergen, Alleġt. 41, N-5007 Bergen*.

Breivik, A. J., & Mjelde, R. (2001b). Obs-98 survey: Final report western continental profiles. *Report*, *Univ. of Bergen, Alleġt. 41, N-5007 Bergen*.

Breivik, A. J., Verhoef, J., & Faleide, J. I. (1999). Effect of thermal contrasts on gravity modeling at passive margins: Results from the western Barents Sea. *Journal of Geophysical Research: Solid Earth*, *104*(B7), 15293-15311. https://doi.org/10.1029/1998jb900022

Brozena, J. M., Childers, V. A., Lawver, L. A., Gahagan, L. M., Forsberg, R., Faleide, J. I., & Eldholm, O. (2003). New aerogeophysical study of the Eurasia Basin and lomonosov ridge: implications for basin development.(Author Abstract). *Geology*, *31*(9), 825. https://doi.org/10.1130/g19528.1

Clerc, C., Jolivet, L., & Ringenbach, J.-C. (2015). Ductile extensional shear zones in the lower crust of a passive margin. *Earth and Planetary Science Letters*, *431*, 1-7. https://doi.org/10.1016/j.epsl.2015.08.038

Curewitz, D., Okino, K., Asada, M., Baranov, B., Gusev, E., & Tamaki, K. (2010). Structural analysis of fault populations along the oblique, ultra-slow spreading Knipovich Ridge, North Atlantic Ocean, 74°30'N-77°50'N. *Journal of Structural Geology*, *32*(6), 727-740. https://doi.org/10.1016/j.jsg.2009.08.011

Czuba, W., Grad, M., Guterch, A., Majdański, M., Malinowski, M., Mjelde, R., et al. (2008). Seismic crustal structure along the deep transect Horsted'05, Svalbard. *Polish Polar Research*, *29*(3), 279-290.

Czuba, W., Ritzmann, O., Nishimura, Y., Grad, M., Mjelde, R., Guterch, A., & Jokat, W. (2005). Crustal structure of northern Spitsbergen along the deep seismic transect between the Molloy Deep and Nordaustlandet. *Geophysical Journal International*, *161*(2), 347-364.

Dumais, M. A., Gernigon, L., Olesen, O., Johansen, S. E., & Brönner, M. (accepted). New interpretation of the spreading evolution of the Knipovich Ridge derived from aeromagnetic data. *Geophysical Journal International*.

Dumais, M. A., Gernigon, L., Olesen, O., Lim, A., Johansen, S. E., & Brönner, M. (submitted). Crustal and Thermal Heterogeneities across the Fram Strait 1 and the Svalbard Margin. *Tectonics*.

Engen, Ø., Faleide, J. I., & Dyreng, T. K. (2008). Opening of the Fram Strait gateway: A review of plate tectonic constraints. *Tectonophysics*, *450*, 51-69.

Engen, Ø., Frazer, L. N., Wessel, P., & Faleide, J. I. (2006). Prediction of sediment thickness in the Norwegian-Greenland Sea from gravity inversion. *Journal of geophysical research*, *111*, B11403.

Faleide, J. I., Tsikalas, F., Breivik, A., Mjelde, R., Ritzmann, O., Engen, Ø., et al. (2008). Structure and evolution of the continental margin off Norway and Barents Sea. *Episodes*, *31*(1), 82-91.

Funck, T., Geissler, W. H., Kimbell, G. S., Gradmann, S., Erlendsson, Ö., McDermott, K., & Petersen, U. K. (2017). Moho and basement depth in the NE Atlantic Ocean based on seismic refraction data and

receiver functions. *Geological Society, London, Special Publications*, *447*(1), 207-231. https://doi.org/10.1144/sp447.1
Gaina, C., Gernigon, L., & Ball, P. (2009). Palaeocene–Recent plate boundaries in the NE Atlantic and the formation of the Jan Mayen microcontinent. *Journal of the Geological Society*, *166*(4), 601-616. https://doi.org/10.1144/0016-76492008-112
Gaina, C., Werner, S. C., Saltus, R., & Maus, S. (2011). Chapter 3 Circum-Arctic mapping project: new magnetic and gravity anomaly maps of the Arctic. *Geological Society, London, Memoirs*, *35*(1), 39. https://doi.org/10.1144/m35.3
Geosoft (2006). GM-SYS profile modeling. Gravity and Magnetic Modeling Software, v. 4.10. *Geosoft Incorporated*, p.116.
Geosoft (2010). Geophysics Levelling System - Processing and Enhancing Geophysical Data Extension for Oasis montaj v7.1 - Tutorial and User Guide. *Geosoft Incorporated*, 70pp.
Geosoft (2014). Geosoft Oasis Montaj extension - GM-SYS 3D Modelling, Feature Sheet, *Geosoft Inc.*
Gernigon, L., Franke, D., Geoffroy, L., Schiffer, C., Foulger, G. R., & Stoker, M. (2019). Crustal fragmentation, magmatism, and the diachronous opening of the Norwegian-Greenland Sea. *Earth-Science Reviews*. https://doi.org/10.1016/j.earscirev.2019.04.011
Glebovsky, V. Y., Kaminsky, V. D., Minakov, A. N., Merkur'ev, S. A., Childers, V. A., & Brozena, J. M. (2006). Formation of the Eurasia Basin in the Arctic Ocean as inferred from geohistorical analysis of the anomalous magnetic field. *Geotectonics*, *40*(4), 263-281. https://doi.org/10.1134/s0016852106040029
Goussev, S. A., & Peirce, J. W. (2010). Magnetic basement: gravity-guided magnetic source depth analysis and interpretation. *Geophysical Prospecting*, *58*, 321-334. https://doi.org/10.1111/j.1365-2478.2009.00817.x
Grad, M., & Majorowicz, J. (2020). Geophysical properties of the crust and upper mantle of the ocean-continent transition in Svalbard area. *Polish Polar Research*, 1-22.
Hermann, T., & Jokat, W. (2013). Crustal structures of the Boreas Basin and the Knipovich Ridge, North Atlantic. *Geophysical Journal International*, *193*, 1399-1414.
Johansen, S. E., Panzner, M., Mittet, R., Amundsen, H. E. F., Lim, A., Vik, E., et al. (2019). Deep electrical imaging of the ultraslow-spreading Mohns Ridge. *Nature*, *567*(7748), 379-383. https://doi.org/10.1038/s41586-019-1010-0
Kent, D. V., & Gee, J. (1996). Magnetic alteration of zero-age oceanic basalt. *Geology*, *24*(8), 703-706. https://doi.org/10.1130/0091-7613(1996)024<0703:maozao>2.3.co;2
Kenyon, S., Forsberg, R., & Coakley, B. (2008). New Gravity Field for the Arctic. *Eos, Transactions American Geophysical Union*, *89*(32), 289-290. https://doi.org/10.1029/2008eo320002
Ku, C. C., & Sharp, J. A. (1983). Werner deconvolution for automated magnetic interpretation and its refinement using Marquart's inverse modeling. *Geophysics*, *48*(6), 754-774. https://doi.org/10.1190/1.1441505
Lim, A., Panzner, M., Dumais, M. A., & Johansen, S. E. (submitted). Crustal Structure and Fluid Circulation across the Mohns Ridge beneath Loki's Castle Hydrothermal Vent Field: an Integrated Geophysical Study. *Geochemistry, Geophysics, Geosystems*.
Ljones, F., Kuwano, A., Mjelde, R., Breivik, A., Shimamura, H., Murai, Y., & Nishimura, Y. (2004). Crustal transect from the North Atlantic Knipovich Ridge to the Svalbard Margin west of Hornsund. *Tectonophysics*, *378*, 17-41.
Mather, B., & Delhaye, R. (2019). PyCurious: A Python module for computing the Curie depth from the magnetic anomaly. *Journal of Open Source Software*, *4*(39), 1544.
Matthews, K. J., Maloney, K. T., Zahirovic, S., Williams, S. E., Seton, M., & Müller, R. D. (2016). Global plate boundary evolution and kinematics since the late Paleozoic. *Global and Planetary Change*, *146*, 226-250. https://doi.org/https://doi.org/10.1016/j.gloplacha.2016.10.002
Mendel, V., Munschy, M., & Sauter, D. (2005). MODMAG, a MATLAB program to model marine magnetic anomalies. *Computers & Geosciences*, *31*(5), 589-597. https://doi.org/https://doi.org/10.1016/j.cageo.2004.11.007

Minakov, A., Mjelde, R., Faleide, J. I., Flueh, E. R., Dannowski, A., & Keers, H. (2012). Mafic intrusions east of Svalbard imaged by active-source seismic tomography. *Tectonophysics*, *518-521*, 106-118. https://doi.org/10.1016/j.tecto.2011.11.015
Minshull, T. A. (2009). Geophysical characterisation of the ocean–continent transition at magma-poor rifted margins. *Comptes Rendus Geoscience*, *341*(5), 382-393. https://doi.org/10.1016/j.crte.2008.09.003
Müller, R. D., Cannon, J., Qin, X., Watson, R. J., Gurnis, M., Williams, S., et al. (2018). GPlates: Building a Virtual Earth Through Deep Time. *Geochemistry, Geophysics, Geosystems*, *19*(7), 2243-2261. https://doi.org/10.1029/2018gc007584
Novatem (2018). Knipovich Ridge airborne survey 2016 (KRAS-16) - Technical Report, 32pp pp.
Oakey, G. N., & Chalmers, J. A. (2012). A new model for the Paleogene motion of Greenland relative to North America: Plate reconstructions of the Davis Strait and Nares Strait regions between Canada and Greenland. *Journal of Geophysical Research: Solid Earth*, *117*(B10). https://doi.org/10.1029/2011jb008942
Ogg, J. G. (2012). Geomagnetic Polarity Time Scale, 85-113. https://doi.org/10.1016/b978-0-444-59425-9.00005-6
Olesen, O., Brönner, M., Ebbing, J., Gellein, J., Gernigon, L., Koziel, J., et al. (2010). New aeromagnetic and gravity compilations from Norway and adjacent areas: methods and applications. *Geological Society, London, Petroleum Geology Conference series*, *7*(1), 559-586. https://doi.org/10.1144/0070559
Parker, R. L., & Huestis, S. P. (1974). The inversion of magnetic anomalies in the presence of topography. *Journal of Geophysical Research (1896-1977)*, *79*(11), 1587-1593. https://doi.org/10.1029/JB079i011p01587
Pérez-Gussinyé, M., Reston, T. J., & Phipps Morgan, J. (2001). Serpentinization and magmatism during extension at non-volcanic margins: the effect of initial lithospheric structure. *Geological Society, London, Special Publications*, *187*(1), 551. https://doi.org/10.1144/gsl.sp.2001.187.01.27
Phillips, J. D. (1997). Potential-Field Geophysical Software for the PC, version 2.2. *USGS open-File Report*, *97*. https://doi.org/10.3133/ofr97725
Phillips, J. D. (2007). Geosoft eXecutables (GX's) developed by the U.S. Geological Survey, version 2.0, with notes on GX development from Fortran code. *U.S. Geological Survey Open-File Report 2007-1355*, 111 p.
Piepjohn, K., von Gosen, W., & Tessensohn, F. (2016). The Eurekan deformation in the Arctic: an outline. *Journal of the Geological Society*, *173*(6), 1007-1024. https://doi.org/10.1144/jgs2016-081
Ritzmann, O., & Jokat, W. (2003). Crustal structure of northwestern Svalbard and the adjacent Yermak Plateau: evidence for Oligocene detachment tectonics and non-volcanic breakup. *Geophysical Journal International*, *152*(1), 139-159. https://doi.org/10.1046/j.1365-246X.2003.01836.x
Ritzmann, O., Jokat, W., Czuba, W., Guterch, A., Mjelde, R., & Nishimura, Y. (2004). A deep seismic transect from Hovgård Ridge to northwestern Svalbard across the continental-ocean transition: A sheared margin study. *Geophysical Journal International*, *157*, 683-702.
Ritzmann, O., Jokat, W., Mjelde, R., & Shimamura, H. (2002). Crustal structure between the Knipovich Ridge and the Van Mijenfjorden (Svalbard). *Marine Geophysical Researches*, *23*(5-6), 379-401.
Sandwell, D. T., Müller, R. D., Smith, W. H. F., Garcia, E., & Francis, R. (2014). New global marine gravity model from CryoSat-2 and Jason-1 reveals buried tectonic structure. *Science*, *346*(6205), 65. https://doi.org/10.1126/science.1258213
Schiffer, C., Peace, A., Phethean, J., Gernigon, L., McCaffrey, K., Petersen, K. D., & Foulger, G. (2019). The Jan Mayen microplate complex and the Wilson cycle. *Geological Society, London, Special Publications*, *470*(1), 393. https://doi.org/10.1144/sp470.2
Searle, R. (2013). *Mid-ocean ridges*, Cambridge University Press.

Skilbrei, J. R. (1992). Preliminary interpretation of aeromagnetic data from Spitsbergen, Svalbard Archipelago (76°–79°N): Implications for structure of the basement. *Marine Geology*, *106*(1), 53-68. https://doi.org/10.1016/0025-3227(92)90054-L
Srivastava, S. P., & Roest, W. R. (1999). Extent of oceanic crust in the Labrador Sea. *Marine and Petroleum Geology*, *16*(1), 65-84. https://doi.org/10.1016/S0264-8172(98)00041-5
Suckro, S. K., Gohl, K., Funck, T., Heyde, I., Schreckenberger, B., Gerlings, J., & Damm, V. (2013). The Davis Strait crust—a transform margin between two oceanic basins. *Geophysical Journal International*, *193*(1), 78-97. https://doi.org/10.1093/gji/ggs126
Sutra, E., & Manatschal, G. (2012). How does the continental crust thin in a hyperextended rifted margin? Insights from the Iberia margin. *Geology*, *40*(2), 139-142. https://doi.org/10.1130/g32786.1
Talwani, M., & Eldholm, O. (1977). Evolution of the Norwegian-Greenland Sea. *Geological Society of America Bulletin*, *88*, 969-999.
Trulsvik, M., Myklebust, R., Polteau, S., & Planke, S. (2011). Geophysical atlas of the East Greenland Basin: Integrated seismic, gravity and magnetic interpretation. *Volcanic Basin Petroleum Research AS, TGS-NOPEC Geophysical Company*
Vogt, P. R., Fruik, C., Jewett, I., Klitgord, K., Vink, G., & Duncan, R. (1986). *Magnetic anomalies of the North Atlantic Ocean*, Geological Society of America.
Vogt, P. R., Kovacs, L. C., Bernero, C., & Srivastava, S. P. (1982). Asymmetric geophysical signatures in the Greenland-Norwegian and Southern Labrador Seas and the Eurasia Basin. *Tectonophysics*, *89*(1), 95-160. https://doi.org/https://doi.org/10.1016/0040-1951(82)90036-1
Voss, M., & Jokat, W. (2007). Continent-ocean transition and voluminous magmatic underplating derived fromP-wave velocity modelling of the East Greenland continental margin. *Geophysical Journal International*, *170*(2), 580-604. https://doi.org/10.1111/j.1365-246X.2007.03438.x
Werner, S. (1955). Interpretation of magnetic anomalies as sheet-like bodies. *Sveriges Geologiska Undersökning, Series C, Årsbok*, *43*(6).
Whitmarsh, R. B., Pinheiro, L. M., Miles, P. R., Recq, M., & Sibuet, J.-C. (1993). Thin crust at the western Iberia Ocean-Continent transition and ophiolites. *Tectonics*, *12*(5), 1230-1239. https://doi.org/10.1029/93tc00059
Zarayskaya, Y. A. (2017). Segmentation and seismicity of the ultraslow Knipovich and Gakkel mid-ocean ridges. *Geotectonics*, *51*(2), 163-175. https://doi.org/10.1134/s0016852117010095

Appendix A: Flight acquisition report NGU

Daily Report

Date	Flight # (Novatem)	Lines flown	km flown	km reflown	Flight time (hr)	*Comments*
30/08/2016	2				3.3	*Compensation calibration (17:36-18:10 UTC)*
01/09/2016	4	1084,1083,1082,1081	***1055.79***		5.0	*Extreme diurnal exceedance on last line (1081)*
07/09/2016	5	1085	***80.00***		1.2	*Partial line; aborted for diurnal*
09/09/2016	6	1079, 1078	***991.20***		4.9	
12/09/2016	7	1085-1092	***1393.11***	80.00	6.1	*Reflown part of 1085*
15/09/2016	8	1077-1076	***1016.14***		5.4	*Unsettled/Active diurnal*
16/09/2016	9	1075,230,125,1081R	***751.64***	294.74	6.3	*Quiet*
22/09/2016	10	1074-1073	***1042.31***		5.4	
06/10/2016	11	1080,1093-1097	***670.33***		4.5	
26/05/2018	14	101-104	***471.08***		6.5	
28/05/2018	15	1001-1002	***770.52***		7.2	
29/05/2018	16	1002-1005	***575.39***		6.8	
31/05/2018	17	FOM			1.5	Calibration test
04/06/2018	18	1006-1007	***647.00***		6.5	partial flights, aborted for weather
05/06/2018	19	1008-1009	***967.88***		7.7	Active diurnal
06/06/2018	20	1010-1011	***998.82***		7.8	
08/06/2018	21	1012-1013	***1052.30***		7.8	
11/06/2018	22	1014-1015	**1075.85**		8.0	
12/06/2018	23	1016-1017	**1099.40**		8.0	
14/06/2018	24	1018-1019	**1122.96**		8.5	
20/06/2018	26	1020-1021	**798.45**		7.1	partial flights, aborted for weather
22/06/2018	27	1022-1023	**910.94**		6.4	partial flights, aborted for weather
27/06/2018	29	120; 1004	**815.62**	*100.00*	7.2	1004 Partly reflown; Active diurnal
28/06/2018	30	112;121,1003;1006-1007	**1105.71**		7.8	Active Diurnal
30/06/2018	31	1069-1072	**1531.87**		8.4	
02/07/2018	32	227-230;1071	**1014.40**		7.7	T230 was fully reflown
03/07/2018	33	1066-1069	**1586.85**		9.1	
06/07/2018	34	1064-1066	**1225.44**		7.3	Active Diurnal
08/07/2018	35	1038-1039	**1144.50**		7.3	Active Diurnal
09/07/2018	36	116-117;1020-1023	**1568.92**		7.4	Active diurnal
10/07/2018	37	118-1005	**833.99**		6.8	
12/07/2018	38	126-1024	**745.26**		6.8	
13/07/2018	39	1061-1064	**1439.12**		8.1	
14/07/2018	40	118;1059-1061	**1420.38**		8.3	
17/07/2018	41	126;1057-1059	**1415.18**		9.0	Active Diurnal
20/07/2018	42	108-110	**947.21**		6.8	Active Diurnal
22/07/2018	43	104-107;1036	**1256.92**		8.6	
23/07/2018	44	1054-1056	**1456.66**		8.7	
25/07/2018	45	1051-1054	**1571.19**		8.9	
26/07/2018	46	1025-1026;114-115;225	**1678.97**		8.9	
30/07/2018	48	1049-1051	**1391.22**		7.2	
31/07/2018	49	124;1027	**909.93**		6.5	
02/08/2018	50	108;1035;1037	**811.10**		7.2	
03/08/2018	51	115;1026;1028-1029	**1543.40**		8.3	
04/08/2018	52	121;1029-1031	**1392.98**		8.1	
05/08/2018	53	1047-1048	**1108.43**		6.4	
10/08/2018	54	111;113;1031;1032	**1392.57**		8.2	
12/08/2018	55	113;1033;1034	**1210.86**		7.8	
13/08/2018	56	115;119;1036;1037	**1045.44**	485.00	7.8	
17/08/2018	57	120;1004	**0.00**	*964.00*	5.9	Active diurnal - reflight only
18/08/2018	58	1051;1058	**0.00**	899.00	7.2	Active diurnal - reflight only
19/08/2018	59	1049;1053;1056;1057	**495.76**	*473.00*	7.9	Active diurnal
30/08/2018	60	122-123	**821.60**		4.9	
31/08/2018	61	1058;1068;108/110	**0.00**	*1043.00*	8.0	reflights
02/09/2018	62	1035;1040;1041	**1048.47**		6.7	
03/09/2018	63	1049;1051;1053;1056-1058	**886.24**	*215.00*	9.8	
05/09/2018	64	1058;1068;108-110;122;123	**899.13**		5.9	
06/09/2018	65	1033;1035;1040-1042;110	**1005.50**	*192.00*	7.9	
07/09/2018	66	1041;1043-1046;1053;108	**694.11**	162.00	5.8	
09/09/2018	67	110,109	**0.00**	*793.00*	3.0	reflights

GEOLOGICAL
SURVEY OF
NORWAY

· NGU ·

Geological Survey of Norway
PO Box 6315, Sluppen
N-7491 Trondheim, Norway

Visitor address
Leiv Eirikssons vei 39
7040 Trondheim

Tel (+ 47) 73 90 40 00
E-mail ngu@ngu.no
Web www.ngu.no/en-gb/